




Review

# A Review on Low-Temperature Protonic Conductors: Principles and Chemical Sensing Applications

Sofia R. Mendes <sup>1</sup>, Geogenes M. G. da Silva <sup>2</sup>, Evando S. Araújo <sup>3</sup> and Pedro M. Faia <sup>1,\*</sup>

<sup>1</sup> CEMMPRE—Electrical and Computers Engineering Department, FCTUC, University of Coimbra, Polo 2, Pinhal de Marrocos, 3030-290 Coimbra, Portugal; uc2002123458@student.uc.pt

<sup>2</sup> Federal Institute of Education, Science and Technology of the Sertão Pernambucano, Petrolina 56314-520, Brazil; geogenes.gil@ifsertao-pe.edu.br

<sup>3</sup> Research Group on Electrospinning and Nanotechnology Applications, Department of Materials Science, Federal University of São Francisco Valley, Juazeiro 48902-300, Brazil; evando.araujo@univasf.edu.br

\* Correspondence: faia@deec.uc.pt

**Abstract:** Proton conductors are ceramic materials with a crystalline or amorphous structure, which allow the passage of an electrical current through them exclusively by the movement of protons: H<sup>+</sup>. Recent developments in proton-conducting ceramics present considerable promise for obtaining economic and sustainable energy conversion and storage devices, electrolysis cells, gas purification, and sensing applications. So, proton-conducting ceramics that combine sensitivity, stability, and the ability to operate at low temperatures are particularly attractive. In this article, the authors start by presenting a brief historical resume of proton conductors and by exploring their properties, such as structure and microstructure, and their correlation with conductivity. A perspective regarding applications of these materials on low-temperature energy-related devices, electrochemical and moisture sensors, is presented. Finally, the authors' efforts on the usage of a proton-conducting ceramic, *polyantimonic acid* (PAA), to develop humidity sensors, are looked into.

**Keywords:** ceramics; hydrogen bonding; protonic conductors; inorganics; humidity sensing; electrical properties



**Citation:** Mendes, S.R.; da Silva, G.M.G.; Araújo, E.S.; Faia, P.M. A Review on Low-Temperature Protonic Conductors: Principles and Chemical Sensing Applications. *Chemosensors* **2024**, *12*, 96. <https://doi.org/10.3390/chemosensors12060096>

Received: 24 April 2024

Revised: 27 May 2024

Accepted: 30 May 2024

Published: 2 June 2024



**Copyright:** © 2024 by the authors. Licensee MDPI, Basel, Switzerland. This article is an open access article distributed under the terms and conditions of the Creative Commons Attribution (CC BY) license (<https://creativecommons.org/licenses/by/4.0/>).

## 1. Introduction

R&D, as shown in recent years, has demonstrated rising interest in proton-conducting materials due to their usage in energy conversion, storage applications, and electrochemical sensors, to mention a couple. Proton-conducting materials that can operate at low temperatures (i.e., that operate without showing behavior degradation at temperatures below 400 °C) and are simultaneously efficient and stable are particularly attractive.

Ceramic semiconductor materials are the first choice for the development of proton conduction devices due to their chemical and structural stability; possibility of use as nanoparticle and nanopore structures, with mixed components and doping; high specific surface area; and high reactivity with the environment and other functional materials.

The conduction mechanism in protonic conductors involves the hopping of H<sup>+</sup> protons through the crystalline structure of the material; the ions' mobility is dominant for the conduction process since H<sup>+</sup> species, due to their small radius, require lower activation energies to move through the atomic structure and existing interfaces [1].

As stated, one of the areas where interest has increased in proton-conducting semiconductors is in energy. The more traditional materials used in developing solid oxide fuel cell electrolytes are oxygen-ion-based and operated in high-temperature ranges between 700 and 1000 °C. At those temperatures, ceramic degradation is one of the main reasons for the limited use of solid oxide fuel cells. Consequently, materials that operate and display structural stability at low or intermediate temperatures (below 400–500 °C) are needed. In addition, water role must also be considered.

Typically, protonic conduction is supported by  $\text{OH}^-$  or  $\text{H}_3\text{O}^+$  ions migrating in an aqueous environment. However, this limits the operating temperature to around  $100\text{ }^\circ\text{C}$  [2]. The goal is instead to achieve conduction by free protons,  $\text{H}^+$ , between stationary host anions. This diminishes the need for molecular water in the structure and allows it to raise the temperature, improve kinetics, and avoid liquid water handling. Consequently, the protons have roles as charge carriers and defect terminators. Actual proton conductors utilize a stationary host structure upon which protons jump from site to site. High-temperature proton-conducting polymers may utilize nitrogen as a proton host. Protons are added by sulfonation or phosphonation, and the materials can operate at temperatures higher than  $100\text{ }^\circ\text{C}$  as they do not depend on water as a proton mediator, unlike standard polymer  $\text{H}_3\text{O}^+$  conductors such as Nafion. Another challenge regarding proton transportation is the strong O–H bond. At high temperatures, protons migrate by repeatedly breaking and making bonds. The host oxide ion lattice must possess sufficient dynamics to temporarily bring the proton of one host close enough to the neighboring one and allow the proton to jump or tunnel over. For this reason, the activation energies of proton and oxide ion conduction in oxides are often similar. Proton-free oxidic materials can also display at high temperatures proton conduction: for this, acceptor-doped oxides, which are charge compensated by oxygen vacancies in the dry state, must be protonated (hydrated).

However, if, due to the availability of a wider range of material candidates, a reduction in the operating temperature is successfully attained, system costs can also be reduced, along with the improvement in long-term durability. In recent years, new proton-conducting materials with enhanced properties at temperatures lower than  $400\text{ }^\circ\text{C}$  (some at room temperature) have been reported in the literature. In this sense, polymer-based protonic solids represent an alternative for the development of new functional hybrid materials that respond to current demands for sensing performance, flexibility, and protonic conduction at temperatures below  $100\text{ }^\circ\text{C}$ . In solid proton conductors with a polymeric matrix, processes involving the production of mixed polymeric membranes and/or the incorporation of metal nanoparticles, mixed metal oxides, carbon nanomaterials, and selective salts and acids can significantly increase the proton conductivity of the membrane to electrochemical applications, such as fuel cells and sensors [3,4]. In these cases, interfacial effects are notable for the improvement in the proton transport process due to the interaction of these materials with water molecules in the environment [4]. A limiting parameter to the use of these polymer matrix devices is the operating temperature, generally  $<100\text{ }^\circ\text{C}$ .

A common thread tying together these reports on low-temperature proton conduction ceramics is the existence of an enhanced grain boundary interfacial area due to the usage of nanometer-sized materials. For instance, the authors of [5] prepared nanostructured yttrium-doped barium zirconate and evaluated its grain and grain boundary protonic conductivity for temperatures between  $0$  and  $400\text{ }^\circ\text{C}$ ; their most important finding was the high protonic conduction observed at temperatures below  $100\text{ }^\circ\text{C}$ . Enhanced interfacial proton conductivity at low temperatures was also reported by Miyoshi et al. [6] for yttria-stabilized zirconia. They observed that interfacial protonic conduction was noticeably higher for grain sizes smaller than  $100\text{ nm}$ , which they attributed to the absorbed water at the grain boundary interfaces, which increased dramatically with decreasing grain size; the same was found by Gregori and co-workers [7] and by Takamura and colleagues [8], for ceria, and by Maglia and his team [9], for titania (which did not show bulk proton conductivity in the intermediate level range). Liu et al. [10] picked a lithium conductor and converted it into a proton conductor by ion exchange at low temperatures. At the same time, Zhou and his equals [11] developed a new electron doping stratagem to produce high-performance  $\text{SmNiO}_3$  perovskite proton conductors for use in low-temperature solid oxide fuel cells.

However, it must be stated that introducing new materials with enhanced proton conductivity also results in the advent of new or enhanced fabrication methods. Room-temperature high-pressure compaction, ultraviolet (UV) laser irradiation, hot pressing, and

high-pressure field-assisted sintering/spark plasma sintering (FAST/SPS) are some of the methods successfully used to produce proton conduction materials [12].

The advantages of high-pressure sintering at room temperature involve fast compaction using low temperatures, grain size stability, and low processing cost [13]. On the other hand, monitoring of the synthesis is required to avoid the phenomenon of cold welding of particles when they are subjected to high pressures [14]. Syntheses with UV radiation and plasma can be used for the rapid formation of active sites in the polymeric matrix. UV radiation can provide subsurface modifications of the material due to its ability to penetrate the bulk, but it can require high energy for the process. Alternatively, plasma-induced polymerization is applicable only for modifications on the surface of the material [15]. Hot pressing is characterized as an environmentally friendly to manufacture protonic conductors. Still, it has the limitation of manufacturing simple shapes with low productivity and high cost [16]. The FAST/SPS process promotes good homogeneity of the grain-size distribution and porosity dependent on the applied pressure [9,16].

Demanding material processing conditions, such as high sintering temperatures and stable atmospheric exposure, prevent proton conductors' large-scale use. Macroscopically, grain boundary impedance in proton conductors can be cut by employing nanosized materials that are easier to sinter or sintered using additives. Consequently, proton conductors' production still imposes solving diverse challenges. Depending on the desired application, they should exhibit some of the following requisites [17]: (a) full gas tightness—to avoid any non-electrochemical gas mixing of anode and cathode atmospheres, the ceramic electrolytes need to be densified at relatively low sintering temperatures. This becomes a critical factor in the co-sintering of two (or more) different functional materials. High sintering temperatures lead to undesirable facilitated migration of cations from one phase to another; (b) high ionic conductivity—the performance of proton conductors is regulated by the Ohmic resistance contribution, which can be minimized either by reducing the thickness of the solid material or by using highly conductive ones; (c) low electronic conductivity—the solid materials should exhibit a wide electrolytic domain boundary with negligible electronic conductivity in both oxidizing and reducing atmospheres. High electronic conductivities originate current flows through the material, causing internal short circuits. This results in considerable efficiency decrease, even for devices yielding superior performance; (d) good thermomechanical compatibility—all materials display dimensional temperature response variation. Therefore, the materials should present thermomechanical compatibility with the joining materials.

So, as is being discussed, proton mobility is highly conditioned by grain boundaries and, consequently, by discontinuities in the hopping trajectories in the vicinity of the grain boundaries, which may increase the overall enthalpy of mobility. The distribution of charge across the grain boundary and the enrichment of effectively positive oxygen vacancies at the intercept between two grains—the grain boundary core—creates a potential relative to the grain interior (known as Schottky Barrier Height). To compensate for this deviation in the charge relative to grain interior and retain electroneutrality, the concentration of other positively charged defects decreases, and negative defects are enriched, originating different conductivities along the grains and grain boundaries (and consequently on their respective activation energies). This was verified by Kjølseth et al. [18], which investigated the specific grain and grain boundary conductivities of  $\text{BaZr}_{0.9}\text{Y}_{0.1}\text{O}_{3-\delta}$  function of oxygen partial pressure and temperature, by impedance spectroscopy combined with the bricklayer model: they have shown that oxygen partial pressure dependencies were indicative of dominating ionic and p-type electronic conduction for the grain interior under reducing and oxidizing conditions, respectively, while the grain boundaries showed an additional n-type electronic contribution under reducing conditions. They established a formulation relating grain and grain boundary conductivities with their respective activation energies, which allowed for the assessment of the space charge layer from the specific grain boundary and grain interior conductivity as a function of temperature.

In general, the mechanisms of interfacial conduction that have been used to describe low-temperature conduction on nanomaterials-based protonic conductors are related to proton transport along the nanostructure. The nanostructure is usually composed of nanograins connected to a hydrated layer, in which interface a pathway for protonic conduction arises (instead of bulk transportation typical of intermediate and high-temperature systems).

The role of interfaces in blocking or enhancing ionic conduction in various solid materials is critical. The two most important interfacial phenomena effects that either enhance or block ionic conduction are the formation of space charges and two-dimensional (2-D) interfacial phases [19]. The first interfacial effect conditioning proton conduction is the formation of space charges, the origin of which is like that of electrical double layers at interfaces between metal electrodes and aqueous electrolytes (similar phenomena have also been discussed and modeled in semiconductor physics for modeling Schottky barriers and p-n junctions). The formation of a space-charge region is caused by the accumulation of net charges at the interface due to the different adsorption enthalpies of the positively and negatively charged defects. The charges in the interface are generally assumed to become adsorbed, which may often have different states or even different effective charges, when compared with their counterparts inside the bulk: once those become chemically connected to the materials, they are assumed to be immobile, even if their counterparts in the bulk and the space-charge zones are mobile carriers, and consequently, the materials exhibit low conductivity. The second major interfacial effect that significantly impacts proton conductivity is represented by the formation and transition of 2-D interfacial phases. The scientific community has recognized the broad existence of a class of impurity-based, nanometer-thick, intergranular films, IGFs, in various oxide and non-oxide ceramic materials. Initially, it was proposed that these IGFs adopt an *equilibrium* thickness on the order of 1 nm in response to a balance among several attractive and repulsive interfacial forces. Thermodynamically, these nanoscale IGFs can be alternatively considered a class of multilayer adsorbates or one special type of 2-D interfacial phases, which can exhibit atomic structures and compositions that are neither observed nor necessarily stable as bulk phases.

All the now-mentioned factors determine the overall protonic conduction of the materials.

In protonic conduction, four charge transport paths are usually considered [7] transportation along grain boundaries, transportation along the surface (due to the proton-enriched layer formed between the pore/oxide interface), transport along the open pores surface covered by a water layer or by open pores filled with water, and proton transfer along the bulk. For high temperatures, i.e., above 500 °C, water absorption is limited near the grain boundaries, so proton conduction occurs mainly by diffusion through the bulk, which displays smaller resistance than the found for grain boundaries.

Below 100 °C, open porosity is a decisive factor regulating protonic conduction due to the possibility of physisorbed water layers formation (on top of the chemisorbed one), which originates additional paths for ions transfer in the system. In resume, protonic conduction at low temperatures depends mainly on the nanostructure (grain size, porosity, etc.) and humidity concentration. Based on these aspects, this work presents a review of proton conductors' principles and applications in low-temperature conditions. In the last section, particular focus is given to humidity sensing applications, where the authors have also been working, reporting their recent efforts.

## 2. Proton Conductors

### 2.1. Origin

The beginning of the academic and industrial attention directed to advanced batteries based on solid electrolyte membranes started with the patent submitted by Dzieciuch and Weber in 1967 [20], associated with a paper of Yao and Kummer [21] (all from Ford Motor Co., Dearborn, MI, USA); in it, the ion exchange properties and high conductivity of beta ( $\beta$ ) alumina ceramics were demonstrated, and they built a Na(Li)/ $\beta$  alumina/Na(Li)Sx

battery, which displayed very-high-density and volume energy, making it possible to power a vehicle electrically.

The first published works on proton conductors date back to 1972 [22] and 1975 [23]. It can be stated that the first steps by the academic community devoted to ion- and proton-conductivity in solid-state materials were due to the first oil crisis in 1973; by then, additional funds were given and used in fundamental research on new solid electrolytes and electrodes for advanced energy conversion and storage devices. The first international conference on fast ion conductors was held at Belgirate (Italy) in 1972 [24,25] in the form of a NATO Advanced Study Institute on 'Fast Ion Transport in Solids, Solid State Batteries and Devices'. Other conferences and meetings were held during the following years. In 1977, Roth and colleagues [26] measured the conductivity of pelletized  $\beta$  alumina samples on  $\text{H}_3\text{O}^+$ , while Colombari et al. [27] measured it on  $\text{H}_3\text{O}^+$ ,  $\text{H}^+(\text{H}_2\text{O})_n$ , and  $\text{NH}_4^+$ . Later, the conductivities of  $\beta$  and  $\beta''$  alumina with different non-stoichiometry and cations were also measured on single crystals and ceramics [27–30].

Attention was focused on improving the physicochemical and conductivity properties of  $\beta$  alumina ceramics with the incorporation of sodium and lithium cations for the construction of electric batteries. These materials were known for their high energy density capacity, which would later enable the development of electric cars. Research at the time also demonstrated the ability of these latter materials to sense hydrogen species concentration (both in water and gas) [31,32]. The studies of improved conductivity of  $\beta$  alumina matrix materials returned values of the order of  $2 \times 10^{-3} \text{ S/m}$  at room temperature. Nevertheless, the area still had a modest number of related studies; attesting to this is the fact that in a book published in 1978 by Hagenmuller and Van Gool [33], among more than 500 pages, only in 4 pages was H diffusion/conductivity addressed.

The second oil crisis in 1979 (when the price of an oil barrel rose from 14 to 40 US dollars) was a relevant global event that boosted the evolution of research on solid-state protonic conductors for electrochemical applications. In 1980, the journal *Solid State Ionics* was created, but the attention given to proton conductors was still short at those times. In 1980 and 1981 were published in the *Journal* the first reports on proton conductors which dealt with potassium hydroxide [34] and with  $\beta$  alumina single crystal conductivity [28]. It must be stated that  $\beta$  alumina usage is very open once ions can diffuse in almost free form along the packed planes in the dense spinel structure [35–37]. Focus was, by that time, given to sodium, lithium, and silver ion conductors; while lithium was considered based on its light weight, sodium was selected due to its good compromise between large availability and electrochemical characteristics, quite like those displayed by lithium. Their potential use in developing energy storage devices and fuel cells was immediately perceived. However, fuel cells were not the pioneer materials used and tested. In 1955, Grubb [38,39] developed polymer membrane-based fuel cells. Later, Forrat et al. [40] tested a perovskite  $\text{AlLaO}_3$  ceramic membrane-based  $\text{H}_2/\text{O}_2$  fuel cell. Already in the 1980s, E.I. DuPont de Nemours & Company started to develop fuel cells for trucks and buses based on a sulfonated tetrafluoroethylene-based fluoropolymer-copolymer [41], commonly known nowadays as Nafion<sup>®</sup>. The National Aeronautics and Space Administration (NASA) of the US government was also another important agency that endorsed the use of Nafion as a polymer–electrolyte fuel cell based on its applications for generating energy in aerospace technologies [42]. Takahashi and colleagues [43] conducted the first systematic investigation of ionic conduction in perovskite ceramics (published in 1980); they evaluated the proton conductivity of lanthanum–yttrium oxide and strontium zirconate.

Presently, their relevance is noticeable once many of the on-market polymer–electrolyte fuel cells for automotive applications are based on perfluorosulfonic acid polymers [42,44–48]. Nevertheless, their development is still ongoing. In general, the increasing demands in this area of research, which include possibilities for the next generation of proton devices, involve the development of miniaturized devices, with low thickness, high chemical and structural stability, and high energy storage and conversion capacities.



## 2.2. Further Impulses

During the last two decades of the 20th century, diverse research communities dedicated more time to proton and ion conductors [49]. Their work on diverse domains, such as those relating to hydrogen bonding, selective ceramics, ion exchangers, and mixed conductors, allowed for further and faster advances in R&D regarding protonic conduction in the first two decades of the 21st century. Figure 1 shows the temporal evolution of scientific publications involving solid-state protonic conductors in the 2010–2023 period. From it, it is possible to observe a transition from the importance given to polymeric electrolytes in the early 2010s to the exploration of solid-state electrolytes from 2015 onwards, with particular attention dedicated to the study of the electrical properties of ceramics. In addition, perovskites were widely cited by the end of the 2010s as potential materials for developing solid-state electrolytes [50].

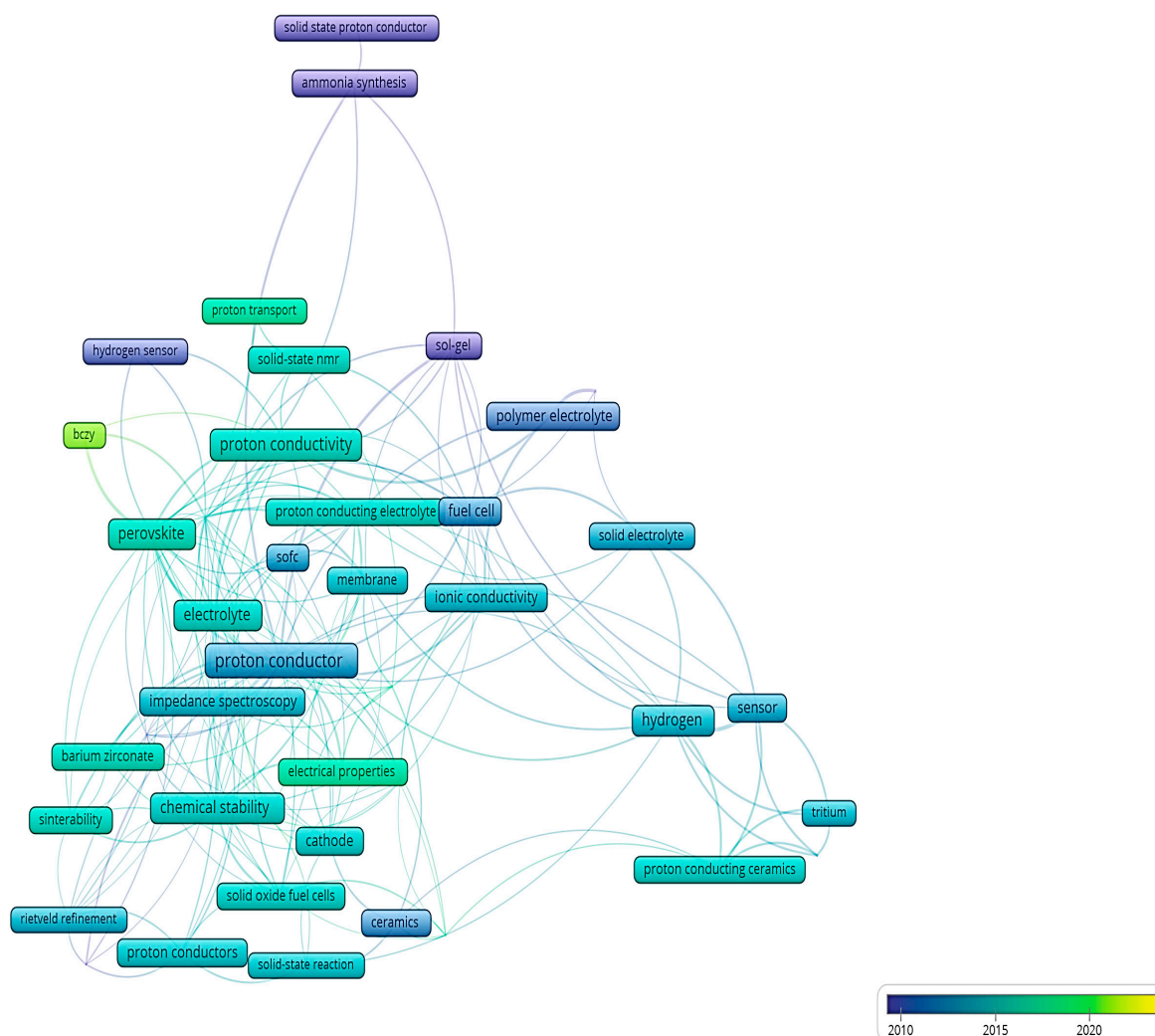


**Figure 1.** Temporal evolution (2010–2023) of publications on solid-state proton conductors ([www.scopus.com](http://www.scopus.com) (accessed on 31 March 2024)).

It is also possible to notice that techniques for physical–chemical analysis of materials, such as nuclear magnetic resonance (NMR), electrical impedance spectroscopy (EIS), and Rietveld refinement, are commonly referred to by researchers in their investigation reports, mainly due to the possibility of clearly determining the species participating in the conduction processes, the conduction types, and the confirmation of the synthesis of previously designed structures.

### 2.2.1. Hydrogen Bonding

Hydrogen bonds represent a crucial factor at the molecular level so that the transfer of protons ( $H^+$  ions) can occur in a given system. This mobility can promote the conduction of protons throughout the bulk and surface of the material and is directly related to the amount of hydrogen bonds due to the interaction with the environment.

Regarding hydrogen bonding, the first works related to their subject were published earlier in the 20th century; however, the ones that started to correlate it with the use and properties of solid proton conductors appeared during the 1980s and 1990s. The book edited by Colombari [51] and the work from Hadzi [52] were somehow precursors of the creation of a conference series entitled ‘Horizons in Hydrogen Bond Research’. By their side, Nagle and Tristram’s investigation was one of the first to focus on the study of hydrogen bonds and the consequent explanation of how protons are transferred across protein membranes in solid/liquid bioenergetic processes [53]. In 1984, Subramanian et al. published the article entitled ‘On the proton conductor  $(H_3O)Zr_2(PO_4)_3$ ’ [54] and used the concept of hydrogen bonds to discuss the conduction properties of this chemical substance in the 25–150 °C temperature range. In 1988, two major contributions to the subject mentioning solid proton conductors were published, one by Kreuer [55] and a second by Novak et al. [56]. In the second, a comprehensive classification of solid-state proton conductors was proposed for the first time. In the 1990s, the work by Kreuer and collaborators focused on presenting inorganic compounds, such as phosphates, sulfates, and ceramic oxides, as potential materials for proton conductivity applications [57–59].

From the 2010s onwards, a growing number of publications focusing on hydrogen bonds to explain conduction by protons in solid-state ceramic materials was noted (Figure 2), following the temporal evolution of solid electrolyte research already highlighted (Figure 1). The depicted data confirms the topic’s importance for advancing related areas for developing new electrolytes for applications in sensors, photocatalysts, fuel cells, batteries, electrochromic devices, and  $CO_2$  converters. In summary, the main characteristic of these solid electrolytes is the conduction of electricity through the diffusion of ions.

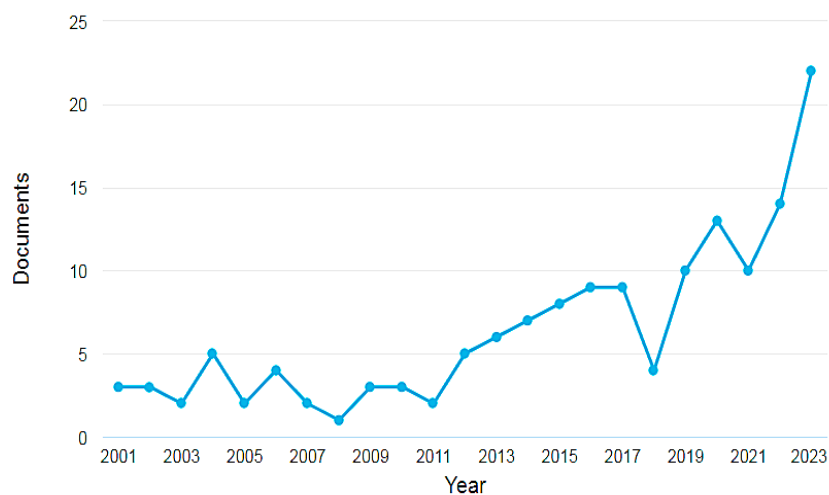


**Figure 2.** Documents by year related to hydrogen bonds in solid-state protonic conductors from 2001 to 2023 ([www.scopus.com](http://www.scopus.com), accessed on 31 March 2024).

### 2.2.2. Ceramic Oxides

Ceramics researchers also paid great attention to the diffusion of protonic species in oxides, which started mainly in the middle of the 20th century. However, the number of studies increased by the end of the century, with the development of technology and consequently on the analysis and measuring equipment. Many aimed to evaluate metal corrosion by water or hydrogen [60,61], while others focused on studying the corrosion of oxides by water or hydrogen [62–64]. Besides being the smallest existing atom, hydrogen can gain or

lose one electron, forming the proton or the hydride ion; consequently, proton detection is complex, and the determination of how they are present in the compound's formula is still often unknown [65]. Nowadays, there are diverse techniques that can be used to detect protons, including direct methods (such as neutron scattering [66], nuclear magnetic resonance [67], and gas chromatography [68]) or indirect ones (like thermogravimetry [69]). All of them are supported by an initial hypothesis regarding the formed/evolved species [70].

Ceramic oxides are widely used as proton conductors due to their properties of high chemical and structural stabilities, porosity, and contact area at the nanometric scale, in addition to high bulk and surface reactivity with selective molecules in the environment, all promoting proton conduction [71]. In addition to the characteristics already mentioned, ceramics such as metals, perovskite, and garnet oxides are widely used in emerging applications of solid-state electrolytes due to their wide electrochemical window, superior safety, and high bulk conductivity at low temperatures [72–74].

Metal oxides are considered crucial because they exhibit excellent electrical/electronic properties, the possibility of being doped with selective donors and acceptors ions using conventional methods, and adjustable band gap; the synthesis of mixed metal oxides with different crystalline conformations may improve proton transport in the resulting systems [74]. Metal oxides synthesized from different combinations of titanium, zinc, aluminum, niobium, vanadium, molybdenum, indium, tin, copper, barium, tantalum, and strontium oxides (and/or with selective dopants) have been used in protonic conductor applications [74–79].

Perovskite oxide solid-state electrolytes, known as garnet oxides, stand out for their excellent optical, electrical, and magnetic properties [80]. A vital characteristic of these oxides, with the general formula  $A_{1-x}A'_x B_{1-y}B'_y O_{3+\delta}$  ( $x$  and  $y \leq 1$ ), is their ability to partially replace cations A and B by metals with varying levels of oxidation ( $\delta$  indicates an additional or missing number of oxygen atoms). This replacement provides vacancies of anions or cations in the crystalline structure of the material, which are directly related to the improvement in proton transport in the system [81]. In addition, garnet oxides present an attractive bright color, good chemical stability, and excellent mechanical and optical absorption properties. They are currently considered as potential replacement materials for liquid electrolytes in lithium batteries, as they enable improved energy density and higher stability of charging and recharging cycles [82,83]; in particular, efforts have been devoted to decreasing the electrical resistance of the lithium/oxide interface [83]. The bibliometric study performed and depicted in Section 2.2, also showed the emergence of the scientific community's interest in  $BaCe_{0.7}Zr_{0.1}Y_{0.2}O_{3-\delta}$  (BCZY) oxide as a protonic conductor in recent years. BCZY is an oxide that can be synthesized by conventional sintering methods, with pre-defined and controlled proportions of its constituent chemical elements, with or without selective additives. The material has high chemical and structural stability and excellent electrical properties, with potential application as an electrolyte in solid-state fuel cells [84–86]. Most recently, Lu et al. [87] reported a novel perovskite oxide ( $SrFe_{0.3}TiO_3$ ) with high conductivity and structural stabilities (at a working temperature range of 420–520 °C) for fuel cell applications. The device showed an energy density greater than 650 mW/cm<sup>2</sup> and stability for more than 12 h, maintaining around 90% of the initial performance in chemical-to-electrical energy conversion tests. In the same direction, the work of Duan et al. highlighted rare earth-doped protonic ceramic electrolytes with high specific surface area and reactivity, capable of maintaining H<sub>2</sub>/electricity round trip converter performance stabilized above 70%, with 1000 h of operating cycles [88]. In fuel cells area, performance advances have been represented by the development of low-thickness protonic ceramic electrolytes (in units of  $\mu\text{m}$ ), structurally dense, chemically stable, and with a high energy density capacity that can reach above 1 W/cm<sup>2</sup> [89].

A common aspect in these recent studies is the search for viable materials and methods for the scalability of these devices for large-scale applications. A notable example of these advances is found in the work of Le et al. [90], where the authors developed a high-performance and scalable bifunctional device, with electrodes and electrolyte (with



20  $\mu\text{m}$ -thick) composed of complex oxides, an extremely high charge density capacity of  $2 \text{ Wcm}^{-2}$  in fuel cell mode, and with 98% Faradic efficiency in electrolysis mode. After 1000 working hours, it was possible to verify very low degradation rates, <4% in the first case, and ~2% under electrolyte mode.

### 2.2.3. Proton Exchangers Membranes

Inorganic proton exchange membranes, such as beta alumina, are one of the most explored solid-state protonic conductors [91]. These membranes are typically semipermeable and designed to act concomitantly as barriers for reactants, such as oxygen and hydrogen molecules. Presently, other ion exchangers are being considered. For instance, zirconium phosphates (ZrP) with diverse structures (amorphous or crystalline) are known for their thermal and hydrophilic stability, ability to incorporate selective ions to improve functionality, and present low production costs while displaying exceptional charge exchange properties [92]. These characteristics are recognized to support the formation of three-dimensional hydrogen bond networks or to permit the inclusion of proton carriers throughout the material structure. Zirconium phosphates can be found in the forms  $\alpha$ ,  $\gamma$  and  $\lambda$ . Proton conductivity is most studied in the  $\alpha$ -ZrP form due to its higher stability and reactivity. Generally, the conductivity in these materials is on the order of  $10^{-4}$ – $10^{-6}$  S/cm at room temperature and high relative humidity. This behavior is directly related to the strong interaction between P-OH bonds and water molecules at the material's surface, which generates a high density of hydrogen bond networks and, consequently, facilitates pathways for proton transfer [93]. Some tin derivatives have also been reported to display excellent ionic conduction properties [94]. Clays like silicon dioxide (silica) and aluminosilicate porous structures exhibit similar behavior, particularly those prepared by the sol-gel method [95,96]. Between silica crystalline and amorphous phases, the latter is highly chosen to produce inorganic membranes due to the possibility of forming structures with mesopores and micropores, whose size distribution can be tuned, for instance, using the parameters of the sol-gel process [97]. Other materials that accommodate hydrates and possess high proton conductivity were also investigated to imitate polymeric membranes, such as Nafion, that present good conductivity at room temperature [43,98]. Actually, one of the main applications for these semipermeable membranes is in the development of energy-related devices such as fuel cells.

### 2.2.4. Mixed Conductors

Composites that display electronic and ionic conductivity have been evaluated for use as energy device electrodes [24]. Compounds containing hydrogen of the type  $\text{H}_x\text{MOn}$  (being M metal elements atoms) have been more intensively evaluated in the last two decades of the 20th century and along the 21st century [99–105]. Besides the compounds mentioned, ferrites and other mixed compounds have also received significant attention during the last decade [106,107]. Nevertheless, electron-insulator polymer membranes are not the only ones to display protonic conduction.

Polyaniline (PANI) is one of the most relevant conducting polymers that have been widely studied due to its unique electrochemical behavior and environmental stability [108–112]; however, relatively low notice was given to its proton conductivity. PANI-based polymers and PANI polymeric salts can be used to form powders, fibers, etc. [113]. Structured layered materials (known as intercalation materials due to the reversible inclusion or insertion of a molecule or an ion into their layered structure) often exhibit proton and electronic conductivity. For instance, carbon can be used to develop advanced capacitors with graphene [114], with a very high surface area per mass unit.

## 2.3. Protonic Conduction

### 2.3.1. Conduction Mechanisms

As already described, under humid conditions, there are four possible proton transport pathways in proton-conducting ceramics [115,116]. For temperatures above 500 °C, water

absorption near the grain boundaries is residual; consequently, once the bulky grain structure possesses smaller resistance than the displayed by the grain boundaries, proton conduction occurs mainly by diffusion through the bulk. Below 100 °C, open porosity is a crucial issue regarding the amplitude of protonic conduction contribution to the overall conduction of the material due to the enhanced physisorption reactions of water that take place along the open pores surface.

In wet environments, proton conduction displays dependency on the working temperature for ceramic materials consisting of simple oxides, fluorite-type or perovskite-type oxides. Three distinct contributions to protonic conduction can be identified (each corresponds to predominant proton conduction), each one tied to the differences observed regarding the form water molecules are chemically and physically adsorbed and consequently become bound to the surface of the oxides [12]; (1) the first contribution takes place for temperatures below 50 °C, and is originated by water molecules physical adsorption; (2) the second contribution is originated when hydrogen bonding competes with water physisorption, in the temperature range in between 50 and 150 °C; (3) the third contribution arises from the moment chemical adsorption prevails, and for temperatures between 150 and 400 °C [117]. Due to the apparent negative activation energy, the first two mentioned contributions are due to the compelling correlation between water adsorption and temperature in the ranges mentioned.

The third contribution, which, as stated, only occurs for temperatures higher than 150 °C, is described by the Grotthuss chain mechanism [118], in which the protons strongly interact with nearby electrons possessing electronegativity like the observed for oxygen ions. Proton transport is an energy-activated hopping process that requires breaking and restoring oxygen/hydrogen, O–H, bonds. However, the materials' total conductivities also strongly depend on their microstructure, which determines charge transport characteristics of bulk and grain boundaries and conduction through interfaces, such as the ones between the material and measuring electrodes.

Following this mechanism, water molecules dissociate into hydroxyl groups ( $\text{OH}^-$ ) and protons ( $\text{H}^+$ ); while hydroxyl groups are incorporated into oxygen vacancies, protons form covalent bonds with lattice oxygen.

Regarding proton hopping, not only the Grotthuss mechanism but also the vehicle one is involved in the charge transfer process; see Figure 3 [119]. In this mechanism, protons do not migrate as  $\text{H}^+$  but as  $\text{H}_3\text{O}^+$ ,  $\text{NH}_4^+$ , etc., bonded to a “vehicle” such as  $\text{H}_2\text{O}$ ,  $\text{NH}_3$ , etc. The “uncharged” vehicles move in the opposite direction. Hopping of proton arises from one  $\text{H}_3\text{O}^+$  to quickly rotating nearest water molecules. This mechanism is not in favor of the fact that  $\text{H}_2\text{O}$  is not a free rotator, but it has tetrahedral hydrogen bond involvement. Nevertheless, the overall proton conductivity due to this mechanism is strongly dependent on the vehicle diffusion rate.

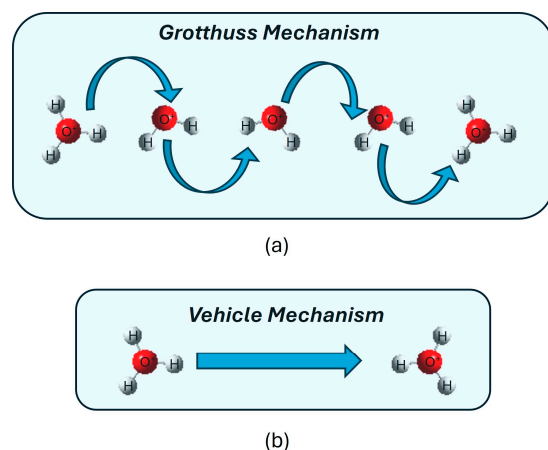


**Figure 3.** Illustration of ion transfer mechanisms in proton conductors: (a) Grotthuss mechanism—protons move along hydrogen bonds; (b) vehicle mechanism—protons move with the aid of a moving “vehicle”.

Improved protonic conduction can be achieved by increasing the number of proton carriers on a material that can be regulated by interacting counterions, such as  $\text{H}_3\text{O}^+$  or  $\text{NH}_4^+$ , with the compound structure: these counterions will form additional hydrogen bonds with the water or other constituents of the compound, creating proton-conducting pathways composed of hydrogen-bond networks. Regarding the Grotthuss conduction mechanism contribution, typically, the ion produced by oxidation in the anode adheres to a water molecule and provisionally creates an  $\text{H}_3\text{O}^+$  ion: then, another proton from the same ion moves to another water molecule, originating one more  $\text{H}_3\text{O}^+$  ion. So, this “continuous” movement of  $\text{H}_3\text{O}^+$  ions contributes significantly to the overall protonic conduction. For vehicular contribution, anion mobility depends on the dissociation of the cationic group: so, higher dissociation rates lead to increased ion mobility and greater conductivity. Consequently crystalline  $\text{NH}_4^+$  interactions (ionization) augment the overall conduction.

### 2.3.2. Interfacial Conduction Mechanism

Lately, large amounts of time and effort have been allocated to developing materials possessing high protonic conductivity, particularly nanostructured ones [120].

The crystal structure is regarded by many as the most important parameter in ionic motion, including both mobility and concentration of ionic charge carriers. Accordingly, the structural effects in the grain boundaries are readily considered since uncompensated bonds in the grain boundaries core cause the electrochemical potential of the ions to result in different defects from the bulk and offer a more open structure between the misaligned adjacent grains. Thus, grain boundaries conduction of ionic charge carriers can be greater than the bulk diffusion through the grains. Regarding the space charge effect, it has been demonstrated that the ionic charge carrier depletes and accumulates in the vicinity of the grain boundaries cores (also named structural transitions), which structurally differs from the bulk: such depletion or accumulation is attributed to the existence of excess charge in the core, which is inevitably formed due to thermodynamic differences between it and the bulk.

Several nanostructured materials have been investigated to enhance protonic conduction at low temperatures [117,121–123]. However, the differences between the conductivity in simple oxides and the complex nanostructured materials are low at low temperatures. Nevertheless, nanocrystalline materials display a high hydration behavior at those lower temperatures (below 50 °C); consequently, adsorbed water molecules at the material surface and the grain boundaries form physisorbed water layers that become paths for proton transport [5]. Therefore, the transition of the conduction mechanism around is correlated with the capillary condensation of water molecules.

Besides the overall interfacial contact area increase, surface terminations and structural features are also important factors to consider regarding proton conduction enhancement. Taking Yttria Stabilized Zirconia, YSZ, as an example, for temperatures below 50 °C, zirconium and oxygen atoms act as Lewis acid and base sites, respectively [124]. Adsorbed water dissociates on the surface of the zirconium-containing structures and forms hydroxyl groups on the surface, which favor proton transport (it was demonstrated that the (111) surface of YSZ enhances dissociative adsorption of water [125]). So, the features of hydroxyl and  $\text{H}_2\text{O}$  molecules interacting with the surface of zirconium nanostructured oxides facilitate proton conduction. Also, in opposition to micrometric-sized grains, nanosized ones tend to enhance water absorption and dissociation processes due to the participation of disordered surface bonds, which leads to the increase in proton conduction at room temperature.

Raz et al. [126] also reported protonic conduction in porous YSZ with a surface-conduction mechanism. They demonstrated that the physisorption reaction dominantly takes place at low temperatures (<100 °C), and the chemisorption reaction dominantly takes place at high temperatures (>100 °C). In the literature, other metal oxides were reported to display similar behavior by forming single or multi-observed water layers, including

$\text{Al}_2\text{O}_3$ ,  $\text{TiO}_2$ ,  $\alpha\text{-Fe}_2\text{O}_3$ , and  $\text{SiO}_2$  [127–129]. Anderson and Parks [129] discussed protonic conduction on silica surfaces; they stated that it was due to adsorption isotherms that are formed by freely vibrating hydroxyl groups offering the strongest surface adsorption sites.

### 2.3.3. Structure Influence

Malavasi et al. [130] stated that nanoscale materials exhibit enhanced properties, where grain boundary interfaces dominate, correlated with the short diffusion lengths and high-density interfaces due to size effects. It is recognized that both bulk and grain boundaries contribute to the total protonic conductivity; consequently, materials' microstructure considerably impacts their electrical properties.

Ionic charge transportation in protonic conducting ceramic materials exhibiting micron-size grains is regulated by the grain boundaries, which act as a barrier opposing the transport of ions in polycrystalline materials. However, the size and structure of the grain boundaries can be tailored, and consequently, the way protons are transported at and through the interfaces, especially at low temperatures. Indeed, the controlled fabrication of nanodomains in the materials allows them to possess a high density of interfaces with short diffusion lengths, giving origin to enhanced conduction characteristics [130,131]. In the literature, there are several examples of the assessment of nanostructured materials that might exhibit enhanced low-temperature protonic conduction. Miyoshi et al. [6] reported the fabrication of nanostructured YSZ with grain sizes smaller than 100 nm, exhibiting remarkable interfacial protonic conduction that increased with the decrease in grain size. Haile and colleagues [132] investigated samples of  $\text{BaCe}_{0.85}\text{Gd}_{0.15}\text{O}_{3-\delta}$  and used the sintering temperature to control the grain size; they looked for the influence of grain size on grain boundary electrical properties. They used a 'brick layer model' to estimate the grain and grain boundary conductivities; the obtained results indicated that the grain boundaries are significantly more resistive than the bulk in barium cerate. Kim et al. [133] investigated the resistivity of nano YSZ with different grain sizes in a fully wet atmosphere. For temperatures higher than 200 °C, the proton transport was insignificant compared to oxygen-ion transport; however, they observed that the nano-Yttria Stabilized Zirconia becomes a proton conductor below 120 °C. They observed that the total resistance decreases significantly as grain size decreases, confirming the grain boundary interface's importance in enhancing proton conduction at low temperatures in the nano-YSZ.

## 2.4. Proton Conductors Applications

Solid-state proton conductors are vital in many technological domains and applications, including hydrogen and humidity sensors, membranes for water electrolyzers, and energy-related devices such as fuel cells. In the following sections, the authors provide an overview of the efforts carried out by researchers in the more relevant domains of application of solid proton conductors and summarize their work in the last couple of years regarding moisture sensing using *polyantimonic acid* (PAA).

### 2.4.1. Energy-Related Devices

The technology of fuel cells that use hydrogen as fuel, operating at temperatures below 100 °C, is nowadays well developed [43,134,135]. The protonic conducting membrane that separates the electrodes must be very thin but hydrogen impermeable for efficient fuel cells. The membranes must also display conductivities above  $10^{-2}$  S/cm and resist oxidation reactions.

Most fuel cells are based on Nafion or Nafion-like membranes; they exhibit high chemical stability and proton conductivity. Concerning the fuel used in the cells, for temperatures below 100 °C, hydrogen is a common choice. However, methanol is a very promising and appealing choice, envisaging fuel cell usage in electric cars. In recent years, efforts have been committed to developing less expensive membranes than Nafion-based ones. However, once high protonic conduction, as well as a low level of chemical instability to oxidation reactions, are required, the advances have been small; nevertheless, promising

results have been obtained with non-fluorinated polymers [136–139], with zirconium sulfophenyl phosphonates [140,141], and with polyantimonic acid (PAA) [142,143].

Some researchers have been working on proton-conducting membranes but following a parallel approach, and they have evaluated perfluorinated ion exchange membranes. These membranes are different from conventional ion-exchange ones once they are thermoplastic polymer-based. Perfluorinated ionomer membranes take advantage of their crystalline domains to avoid dissolution; so, the variation in the temperature and water content of the polymers is likely to cause the variation in the proton's transportation (already observed experimentally). It is presently recognized that the dispersion of hydrophilic nanoparticles in the polymers alters the size of the ionic clusters and their hydrophilic interconnections. Consequently, the interest in hybrid membranes has been extended to systems based on other ionomers such as silica, titania, or antimonic acid [41,144].

Debbarma and collaborators [145] developed a flexible polyelectrolyte of Polyvinylidene fluoride (PVDF) and poly(2-acrylamido-2-methyl-1-propane sulfonic acid) (PAMPS) as a protonic conducting membrane. The authors showed that the conductivity of the composite increases (because of the increase in proton mobility) with increasing excitation frequency and the proportion of PAMPS in the final material, in the range of 20 Hz to 20 MHz. The best proton conductivity results (0.238 mS/cm) and sensing properties (variations in applied force, pressure, or stress) were obtained for the 40/60 bulk PVDF/PAMPS composite. Other work has focused on the study of proton-conducting electrolytes based on poly(ethylene oxide) (PEO) and poly(methylmethacrylate) (PMMA) under the inclusion of salts and acids for the development of electrochemical cells operating at room temperature [3]. Another example involves a composite electrolyte of polystyrene sulfonic acid (PSSA), zirconium (IV) tungstophosphate (ZWP), and sulfonated poly(vinylidene fluoride) (SPVDF), SPVDF-ZWP-PSSA, was produced as a protonic exchange membrane fuel cell. The nanocomposite showed a proton conductivity of ~3.9 mS/cm. In addition, tests using direct methanol fuel cells showed that the best performance of the SPVDF-ZWP-PSSA membrane was obtained at an operating temperature of 60 °C, with a power density of ~20.0 mW/cm<sup>2</sup> [146]. The use of proton-conducting ceramics in energy conversion and storage applications represents a significant segment of the advances in the domain of solid-state protonic conductors [88,89,147,148]. In the literature, it is possible to find representative studies on the advancement of the use of proton-conducting fuel cells. In 2019, an electrochemical cell for reversible hydrogen (H<sub>2</sub>)-electricity-H<sub>2</sub> conversion (in which the reaction occurs in both directions) was developed using a solid solution of barium kerate-zirconate co-doped with yttrium (Y) and ytterbium (Yb) as an electrolyte, and metal oxide electrodes [88]. The novel system provided a Faradaic efficiency greater than 90%, with an overall electricity-to-H<sub>2</sub> conversion efficiency greater than 97% at 600 °C. H<sub>2</sub>-electricity-H<sub>2</sub> cycles showed stabilized conversion efficiency at approximately 75% even after 1000 operating hours.

Protonic materials also have the potential for energy storage applications as they can be developed with high energy density capabilities in their bulk. Thus, they can convert surplus electricity into chemical energy or vice versa. Another positive characteristic of this type of electrochemical cell is that the storage capacity does not depend only on its dimensions since the chemical fuel can have its volume reduced by pressure for adequate storage in external tanks for an indefinite time. In this perspective, Ann's group manufactured protonic conducting fuel cells with one of the highest energy density capabilities ever obtained up to that time [89]. The authors recorded values around 1.30 W/cm<sup>2</sup> and 0.53 W/cm<sup>2</sup> for temperatures of 600 and 500 °C, respectively, using a BaCe<sub>0.55</sub>Zr<sub>0.3</sub>Y<sub>0.15</sub>O<sub>3-δ</sub> (BCZY3) ceramic film (5 × 5 cm<sup>2</sup> in area, and <5 μm in thickness) as electrolyte. The system exhibited a surface area ohmic resistance of 0.09 Ω/cm<sup>2</sup>, delivering power of up to ~21 W in each cell.

In addition, Xing et al. [149] reported the enhancement of proton conduction of the widely known BaZr<sub>0.8</sub>Y<sub>0.2</sub>O<sub>3</sub> (BZY) (generally below 0.1 S/cm) from the formation of semiconductor-ionic heteronanostructures from Ceria (CeO<sub>2-δ</sub>/BZY) for applications



as an electrolyte in solid oxide fuel cells. The authors verified much higher values of proton conductivity (0.23 S/cm) and power (0.845 W/cm<sup>2</sup>) at ~500 °C for the CeO<sub>2-δ</sub>/BZY structure compared to the BZY sample under the same conditions. At a similar working temperature, a SrFe<sub>0.3</sub>TiO<sub>3</sub> (SFT) protonic fuel cell was obtained with energy density capabilities of 0.65 W/cm<sup>2</sup> and current density of 1.14 A/cm<sup>2</sup> as a potential material for the conversion of chemical energy to electricity [87].

In 2017, Gao et al. [4] developed BaCe<sub>0.7</sub>Zr<sub>0.1</sub>Y<sub>0.1</sub>Yb<sub>0.1</sub>O<sub>3-δ</sub> (BCZYyb) nanocrystalline mixed oxide membranes as new materials with improved proton conductivity at working temperatures ≤300 °C. The results indicated excellent surface mobility of protons in the membrane as a combined result of its interfacial (surface and grain boundaries) and bulk effects. At low temperatures, this membrane interface was hydrated with water chemisorbed and physisorbed layers, including free H<sub>2</sub>O, hydronium ions (H<sub>3</sub>O<sup>+</sup>), and surface hydroxyl species. This behavior differs from the usual interfacial blocking effect observed in ionic conductors at high temperatures. Thus, the authors concluded the study by indicating that, at 300 °C, this projected interface is an additional means for proton transport, which indicates the material's better performance for applications such as low-temperature protonic fuel cells.

In another relevant study, Jensen et al. [147] developed a new large-scale storage method combining the use of reversible electrochemical cells based on protonic oxides and the use of subterranean storage tanks for carbon dioxide and methane gases. The authors noted a high efficiency of electrical energy storage and a kW/h cost similar to that required by pumped hydro technologies. Tarasova and collaborators [148,150,151] produced layered perovskites based on rare-earth-doped BaLaInO<sub>4</sub>, using barium carbonate (BaCO<sub>3</sub>), indium(III) oxide (In<sub>2</sub>O<sub>3</sub>) and lanthanum(III) oxide (La<sub>2</sub>O<sub>3</sub>) as primary reactants. The novel proton-conducting materials, neodymium (Nd)-, praseodymium (Pr)-, and gadolinium (Gd)-doped BaLaInO<sub>4</sub> are presented as potential proton-conducting fuel cells. It was shown that the production of these nanomaterials by calcination above 1000 °C was essential for obtaining stable crystalline organizations that favored the proton concentration and mobility under humid air at low temperatures (below 400 °C), with proton conductivity values higher than those obtained for samples without the use of dopants (about 18 times higher for Pr-doped BaLaInO<sub>4</sub>). From the observed results, the authors concluded the potential of these novel electrolytic materials for converting the chemical energy of H<sub>2</sub> to electrical energy.

#### 2.4.2. Sensor Devices

Developing sensing devices with increased sensing capabilities (sensitivity, selectivity, limit of detection, repeatability, etc.) is vital in many private, public, commercial, and industrial domains (such as houses, public buildings, shops, and factories).

Detecting and monitoring air-containing species (for instance, pollution for health control purposes) is common to all locations mentioned, displaying an increasing and urgent search for improved solutions. So, the demand for specific gas sensors is huge. Today, it is common knowledge that protonic conductor membranes that are highly permeable to hydrogen can be used to fabricate sensors. For instance, pellicular zirconium phosphates are good proton conductor candidates for usage in some types of sensors; they display good thermal stability up to 350 °C. Pellicular zirconium phosphate-based sensors can detect hydrogen in the air at low concentrations (up to 10<sup>-6</sup> ppm) [152]. However, using proton conductor materials for sensing applications is typically limited to hydrogen detection/measuring applications. Regardless, highly sensitive amperometric sensors for O<sub>2</sub> [153], CO [154], NO, and NO<sub>2</sub> [155] have been developed.

In the last decade, studies on using proton-based conducting materials for sensing purposes have accelerated and have been reported in the literature. Zhao et al. [156] developed a humidity-assisted sensor for ammonia detection in exhaled air based on hydrophilic polymers. They used as a starting point their previous studies [157] and Li and colleagues' [158] work; in both, it was observed that adsorbed water molecules could

form proton-conductive paths that allowed ion migration and that species and the content of the ionizable group influenced the conductivity of the humidity-sensitive gel. Their explanation for the humidity-enhanced effect in ammonia is as follows: (1) the gas-sensitive films start by physically adsorbing a layer of water molecules; (2) then, due to interactions between water and ammonia molecules, strong hydrogen bonds are formed, resulting in increased ammonia adsorption by the previous physisorbed water layer; (3) subsequently, the adsorbed ammonia dissolves and ionizes into  $\text{NH}_4^+$  and  $\text{OH}^-$ ; (4) last, the migration of  $\text{NH}_4^+$  and  $\text{OH}^-$  along the physisorbed water layer leads to a decrease in resistance.

In 1991, Iwahara et al. [159] developed the first hydrogen sensor based on proton-conducting ceramic materials. For their work, a  $\text{BaCe}_{0.9}\text{Nd}_{0.1}\text{O}_{3-\delta}$  composition was evaluated in an  $\text{H}_2$ , Pt | SCY | Pt,  $\text{H}_2$  + Ar concentration cell type. The obtained experimental data indicated that unipolar proton transport in reducing atmospheres occurred for temperatures below 200 °C and above 1000 °C. Using a Pt reference electrode, the sensor was characterized in atmospheres where a wide range of  $\text{H}_2$  partial pressures ( $10^{-2}$  to 1 atm) were set; it showed good accuracy and high-speed response.

More recently, Okuyama et al. [160] evaluated as a hydrogen sensor an Mn-doped  $\text{CaZrO}_3$ -based galvanic cell; they tested wet  $\text{H}_2$ /Ar mixtures using humidified air as a reference atmosphere. They began by investigating the transport nature of  $\text{CaZr}_{0.995}\text{Mn}_{0.005}\text{O}_{3-\delta}$  and  $\text{CaZr}_{0.95}\text{Mn}_{0.05}\text{O}_{3-\delta}$  electrolytes, and they found that in wet oxidizing atmospheres, Mn-doped zirconates display mixed proton–electron transport, while in reducing atmospheres, nearly pure proton transport is observed. Based on those observations, they evaluated the possibility of using  $\text{CaZr}_{0.95}\text{Mn}_{0.05}\text{O}_{3-\delta}$  to develop a hydrogen sensor: the obtained experimental results were quite promising.

In their work, Luo and co-workers [161] developed a platform for real-time monitoring of dissolved oxygen in a flowing microfluidic environment. The fabricated Clark-type oxygen sensor used a solid-state proton conductive Nafion matrix combined with polydimethylsiloxane as an oxygen-permeable membrane; cyclic voltammetry and chronoamperometry showed a linear reduction in the sensor current in direct relation with the dissolved oxygen concentration under different flow conditions. Furthermore, they claimed that the improved Clark-type oxygen sensor possessed advantages, such as easy fabrication, flexible configuration, fast response time, and real-time detection capabilities.

For their part, using a simple aqueous solution method, Wang et al. [162] developed a cost-effective proton-conducting material, a water-stable 3D Eu-MOF, and metal-organic framework material,  $[\text{Me}_2\text{NH}_2][\text{Eu}(\text{ox})_2(\text{H}_2\text{O})]\cdot 3\text{H}_2\text{O}$ , which exhibits an extensive hydrogen-bonded network and high proton conductivity of  $2.73 \times 10^{-3} \text{ S cm}^{-1}$  at 55 °C and 95% relative humidity. In the case of more recent studies using solid protonic conductors as electrochemical sensors, it is possible to highlight potential systems for environmental and healthcare applications, such as hybrid membranes of amino-functionalized cuprum encapsulating Brønsted acid doped with chitosan for dopamine detection [163]; metal NPs@MOFs nanocomposite electrodes for simultaneous detection of dopamine and uric acid [164]; perovskite membranes as high-stability hydrogen isotope sensors [165]; composite electrodes of metal nanoparticles (NPs)-decorated reduced graphene oxide (rGO) and chitosan for sensing of usual drugs (such as paracetamol) [166]; and graphene oxide matrix nanohybrid electrodes for sensing pesticide concentrations [167].

#### 2.4.3. Protonic Humidity Sensors (Including Authors' Recent Efforts)

One of the first works on using proton-conducting materials in humidity sensors was carried out by Iwahara's group [168]. They built a galvanic cell of Pt |  $\text{SrCe}_{0.95}\text{Yb}_{0.05}\text{O}_{3-\delta}$  | Pt to mimic the operation mode of a potentiometric humidity sensor. The sensor displayed a linear electrical response function of partial water pressure. Katahira et al. [169] fabricated a humidity sensor with an original design; it consisted of two discs of  $\text{SrCe}_{0.95}\text{Yb}_{0.05}\text{O}_{3-\delta}$  protonic electrolyte glued together by the aid of a high-temperature glass sealant. The sensor was able to estimate water vapor partial pressure. Cobb and colleagues [170] also developed a cell with reversible and blocking electrodes for humidity measurement,

which exhibited a substantial electrical response to moisture at low working temperatures. Miao et al. [171] reported the fabrication of hybrid polymer films of polypyrrole/polyoxometalate (a proton-conducting polyoxometalate) with different thicknesses, prepared via the co-electrodeposition of free pyrrole monomers with metal oxide clusters; the observed response and recovery times of 1.9 and 1.1 s, respectively, were determined in the 11–98% relative humidity interval. Based on the performed evaluation after two months, for which the determined response and recovery times were still good, they concluded that the sensor also showed good repeatability. They ascribed the outstanding sensing of the polypyrrole to the synergistic effect of the proton acid doping structure and its oxidation. Zou and colleagues [172] used a natural biopolymer, chitosan, with a unique protonic conductivity. The developed sensor exhibited four orders of magnitude variation in the output when relative humidity increased from 10% to 90%; however, and even more significant, the sensor displayed high stability, repeatability, recoverability, and selectivity to water vapor over ethanol, acetone, and toluene vapors.

Farahani and his team [173] fabricated an innovative self-designed perovskite-based bulk humidity sensor with ceramic support, which they evaluated at room temperature using electrochemical impedance spectroscopy. They observed a direct correlation between the open cavities and the material's conduction; the higher the open porosity, the greater the conduction. By means of electrical impedance tomography, they found that at room temperature, the proton transfer mechanism is dominant and responsible for both charge transfer resistance and kinetically controlled charge transfer (diffusive species) from low and middle to high RH transition. Kalyakin et al. [174,175] fabricated a solid-state amperometric sensor that they evaluated as a moisture sensor under humidified nitrogen and air atmospheres; it was composed of two electrochemical cells based on proton-conducting electrolytes, being one of the cells made of Sc-doped calcium zirconate, while the other is made of Sc-doped barium stannate. Several water vapor partial pressures were used to test the sensor at 500 °C, and volt–ampere relation and calibration curves were obtained. They determined that in nitrogen-humidified atmospheres, the limiting current varied linearly with water vapor partial pressure change, while in humidified air atmosphere, the limiting current could not be reached; however, in humidified conditions, an exception was observed, regarding the limiting current, when they used the Sc-doped barium stannate cell for water vapor partial pressures lower than 0.043 atm.

Medvedev and collaborators [175] also fabricated and characterized a new intermediate-temperature electrochemical cell for examining moisture concentration in gas mixtures. The fabricated electrochemical cell consisted of a diffusion barrier and two electrolytes, one of yttria-stabilized zirconia, with unipolar oxygen ion conductivity, and the other of Sr-doped lanthanum yttrate, with proton transport properties. The tests were performed using the sensor in amperometric mode, and it was able to analyze water vapor partial pressures in gas atmospheres (from 0.001 to 0.1 atm) at intermediate temperatures (400–700 °C). Contrasting with graphene and reduced graphene oxide, graphene oxide, due to its oxygen functional groups, displays proton conductivity and is highly hydrophilic [176]. Guo et al. [177] produced graphene oxide using Hummers' method from natural graphite and prepared moisture sensing films on poly(ethylene terephthalate) substrates employing spin-coating technique. The obtained sensor displayed a decreasing resistance of more than two orders of magnitude when relative humidity increased from 11 to 95%; it showed good linearity and limited hysteresis (around 6%).

The authors of this work have also been studying the usage of protonic conducting materials for humidity-sensing applications. They fabricated pellets of polyantimonic acid (PAA) using different binders and analyzed different compositions; part of the findings have been recently published in the literature [123,178,179]. They started by using as binder a fluoroplastic (grade F-23) and produced and analyzed by electrical impedance spectroscopy (EIS) pellets with 10 and 20% content of binder (designating the samples obtained using PAA and binder in the proportions of 90/10 and 80/20 (wt/wt%), respectively, of 90PAA and 80PAA) [123,178].

The pelletized sensors presented an excellent linear electric response over the RH range, namely the 90PAA sample; see Figure 4, where results obtained for 90PAA response to humidity variation are shown (including the evaluation carried along one year); it was also reported that the sensor displayed almost no hysteresis, a highly satisfactory decline in time response due to aging, and a low fabrication cost. The authors compared samples of pure PAA with those containing the fluoroplastic binder and registered that mixing with the binder enhances the sensitivity of the PAA to humidity [178].

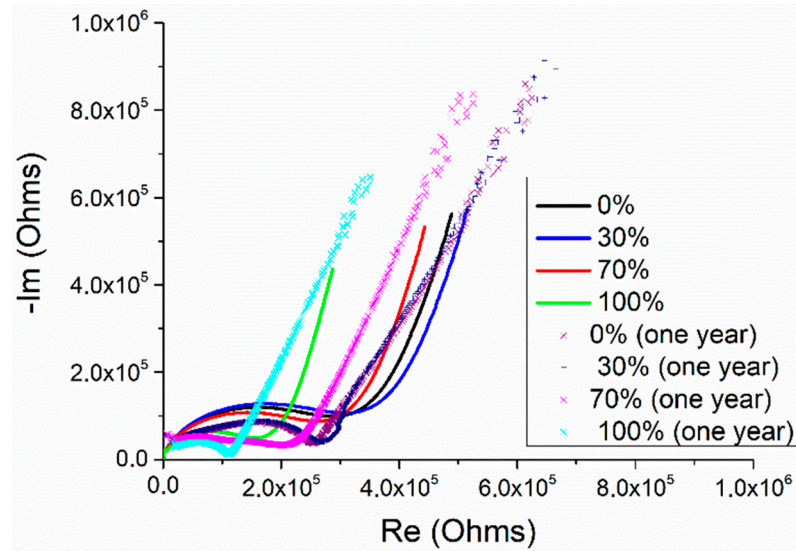


**Figure 4.** Nyquist diagrams for the 90PAA taken over a 1-year time difference for different moisture concentrations (×, first measures; -, measures one year after) [178].

More recently, the authors used another binder, polyvinyl alcohol (PVA), to produce PAA pellets with three different ratios known as PP10 (90% of PAA and 10% PVA), PP15 (85% of PAA and 15% of PVA), and PP20 (80% of PAA and 20% of PVA) [179]. Based on the EIS data obtained, they concluded that PP20 displayed the best electrical response to relative humidity variations, as presented in Figure 5a,b, which display the low and high humidity ranges, respectively).

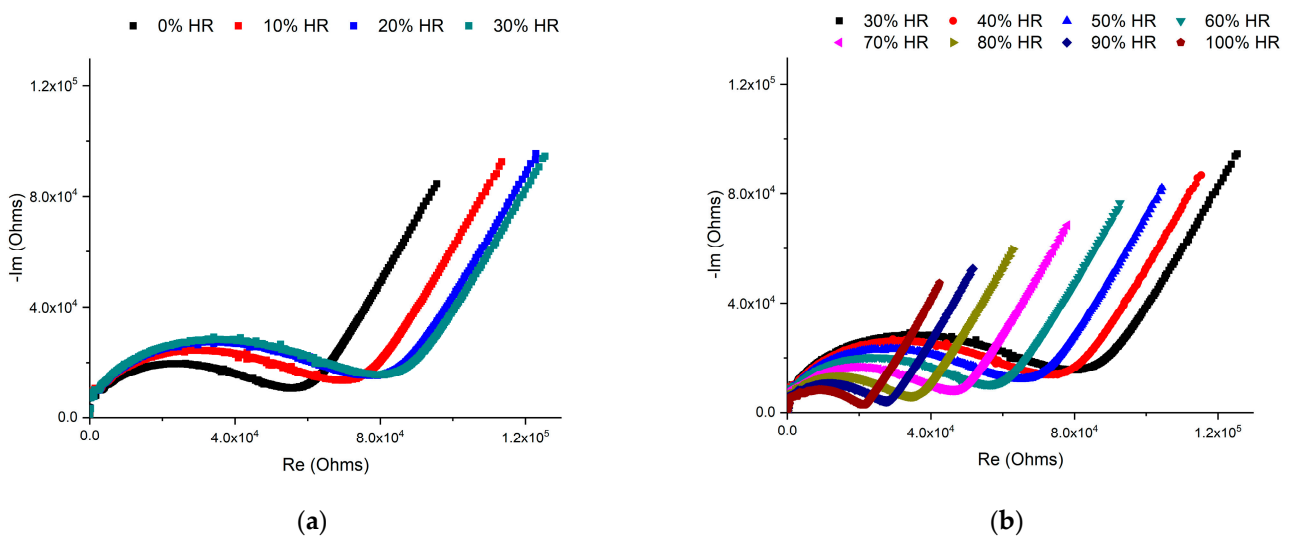


**Figure 5.** RH variation Nyquist plots for PP20 [179] for (a) low humidity ranges and (b) high humidity ranges.

PP20 was also evaluated after three months, demonstrating no appreciable variations in the electrical response to humidity due to sensor aging. Using the impedance data, the authors developed for interpreting that sample electrical response an electrical circuit equivalent model (Figure 6 [179]). The model considered several contributions, where the most relevant contribution, completely visible by looking at the Nyquist plots, is the high ionic contribution (protonic conduction); indeed, the well-defined straight line at high frequencies does not leave space for misinterpretation regarding the proton conduction contribution, which originated by proton hopping resulting from the interaction of the material with water molecules, embodied in the model by a Warburg term.

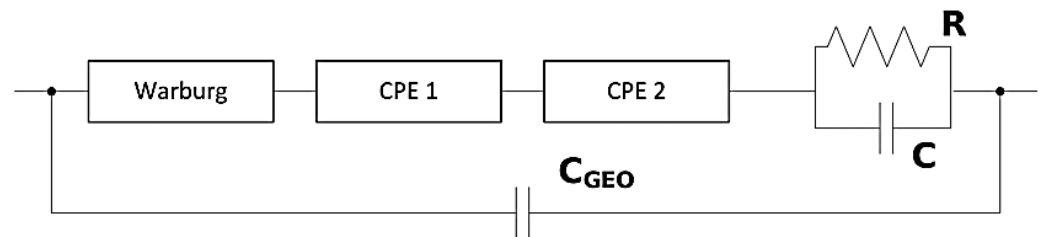


**Figure 6.** Electrical circuit equivalent model [123,178,179].

Figure 7 depicts plots of one example of the experimental and respective model data [179], confirming the model's adequacy to the electrical response of the PP20 sensor (Nyquist and Bode representation).

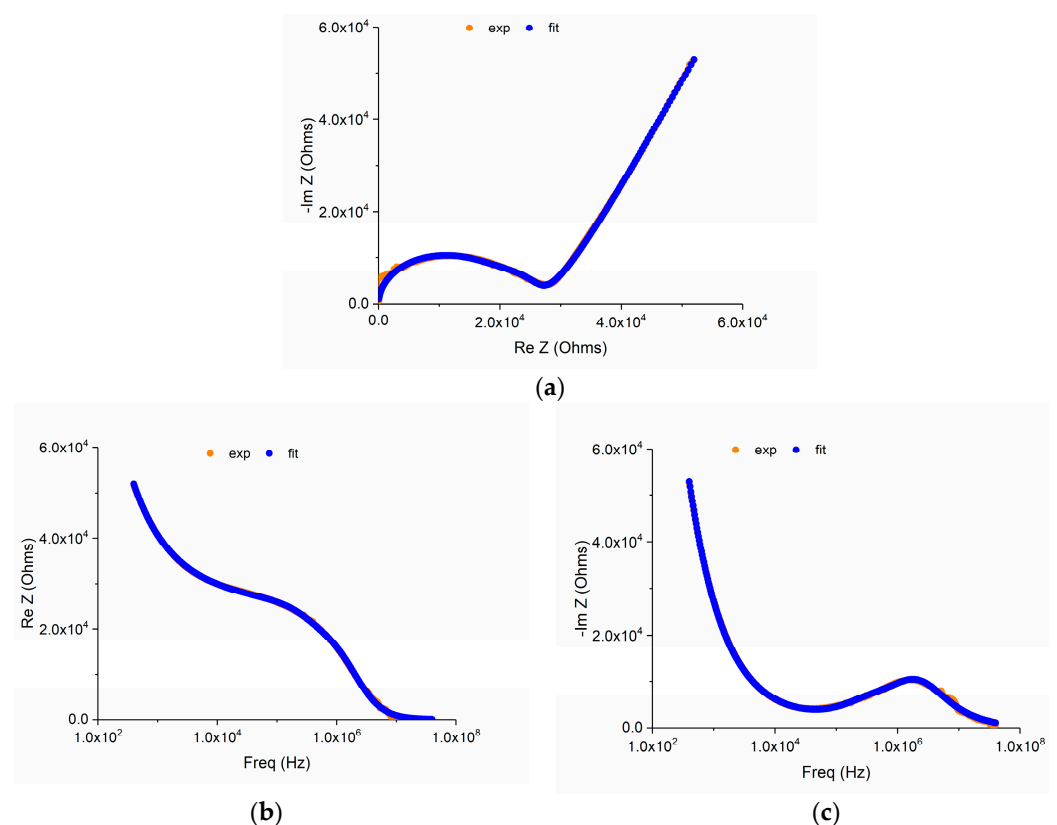


**Figure 7.** PP20 Nyquist and Bode plots (real and reactive components) containing their respective fitted curves, at 90% RH, (a–c), respectively [179].

Presently, once the composition that displayed the best relative humidity sensitivity, combined with low hysteresis, was decided to be sample PP20 (the ones fabricated using fluoroplastic as binder exhibited lower RH sensitivity but almost no hysteresis), the authors decided to further study the PP15 sample; their intents were not only to validate the model



circuit to interpret EIS data but also to perform PP15 evaluation over time and see if it exhibited lower aging than the one shown by PP20 (even if PP20 was the one presenting higher RH sensitivity).

The time evaluation is still not concluded; however, the already-characterized data obtained allowed us to verify that sample PP15; even if it displays lower sensitivity than sample PP20, its stability over time is higher, as can be seen in Figure 8, where time stability for both samples is compared.

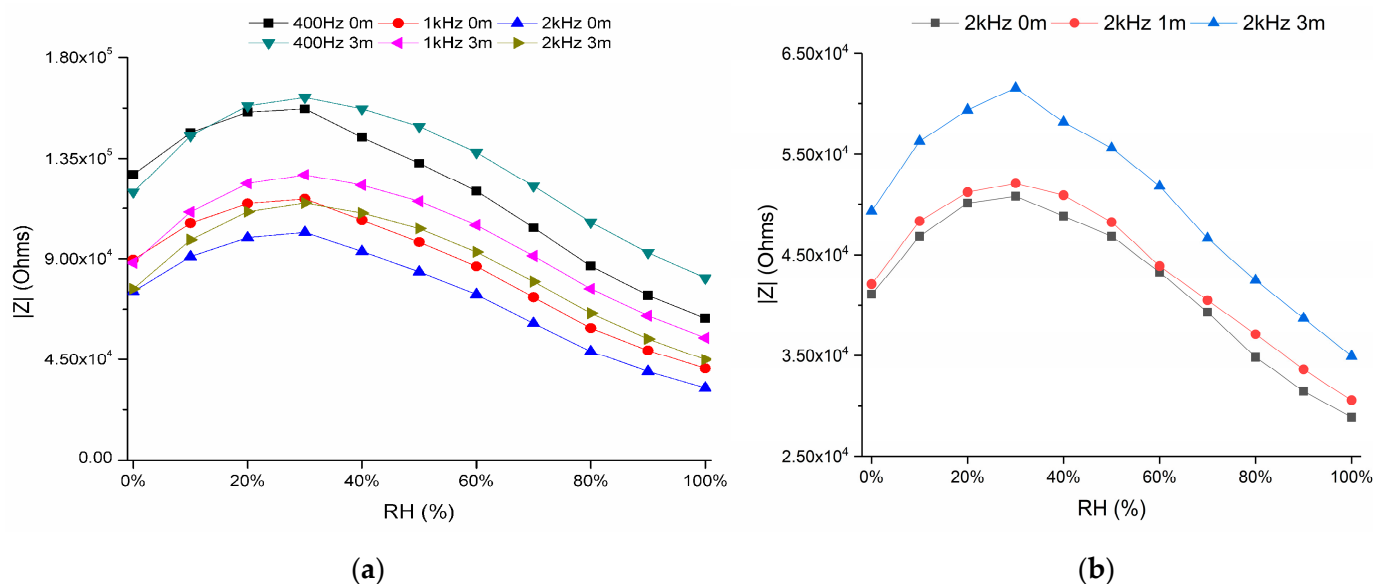


**Figure 8.** Time stability evaluation using the impedance modulus variation with RH and the function of operating frequency (0 m, 1 m, and 3 m stand for the first set of measures, measures conducted one month and three months after the first ones, respectively); (a) PP20 sample; (b) PP15 sample.

Figure 9 displays examples, using Nyquist representations, of the obtained data and respective fits for RH concentrations of 0%, 20%, 40%, 60%, 80%, and 100%. From them, it can be confirmed that the circuit fits the behavior of the PP15 pelletized sensor well in the same way it fitted the remaining fabricated and characterized ones. The most important conclusions were that besides the model's suitability, the Warburg term remains a fundamental element in equivalent electric circuits; indeed, the proton conduction contribution is still dominant and confirmed by the visible straight line in the Nyquist diagrams.

As discussed in the Introduction Section, the conduction mechanism in protonic conductors involves the hopping of  $H^+$  protons through the crystalline structure of the material; this ion mobility is dominant for the conduction process since  $H^+$  species, due to the small radius, require lower activation energies to move through the atomic structure and existing interfaces. In the present ceramic material, as water vapor increases near the material, molecules become chemisorbed and physisorbed; the easy dissociation of physisorbed water produces groups. Charge transport occurs when it releases a proton to a nearby molecule, ionizing it and forming another, resulting in the hopping of protons from one water molecule to another, a process known as the Grotthuss chain reaction; so protonic conductivity is one of the contributions for the overall conductivity of PAA, regarding its usage for moisture detection.

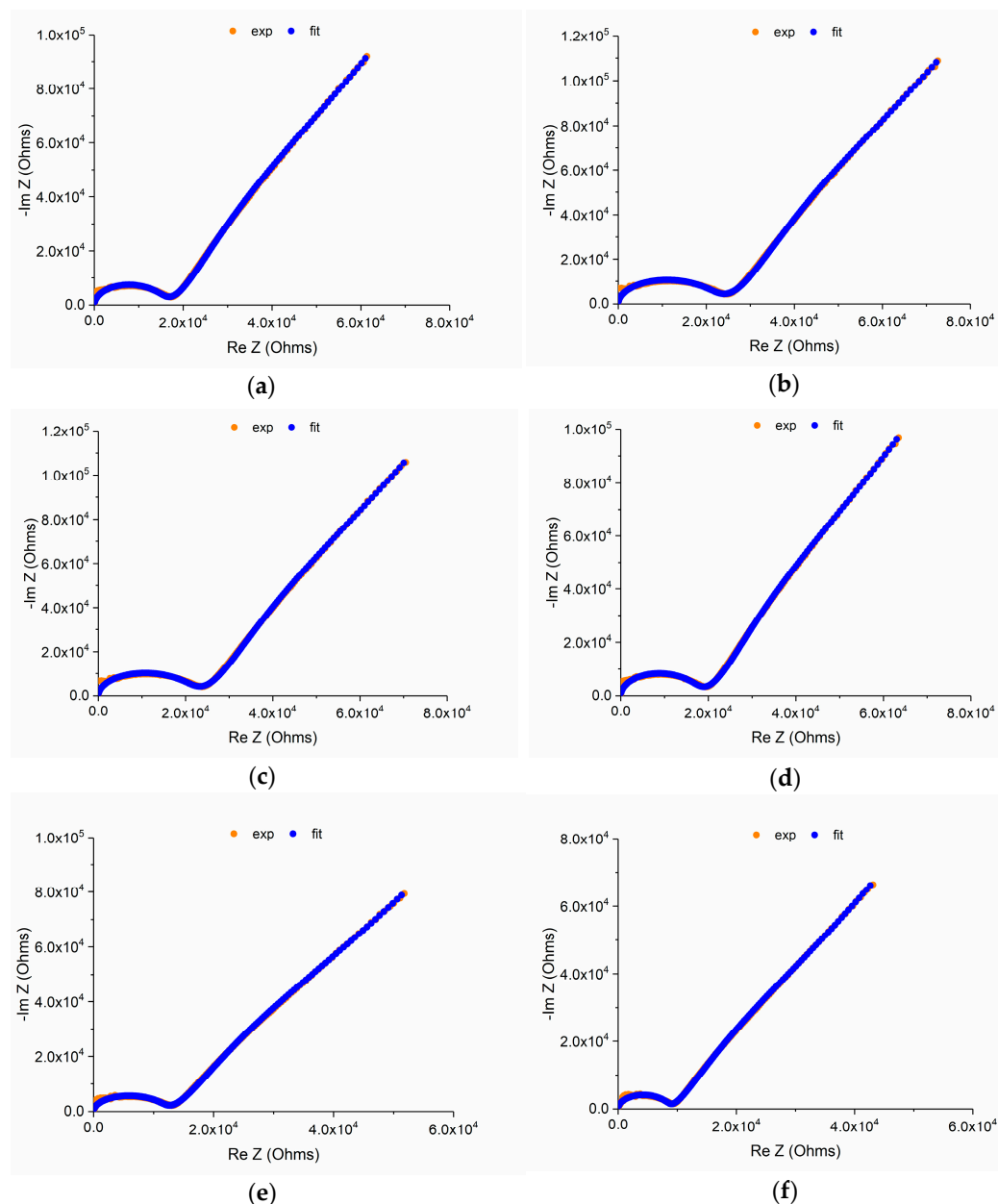


**Figure 9.** PP15 Nyquist plots at 0%, 20%, 40%, 60%, 80%, and 100% RH, fitted curves (a–f), respectively.

### 3. Conclusions

Proton-conducting ceramic materials, possessing crystalline or amorphous structures, which can combine sensitivity, stability, and the ability to operate at low temperatures are particularly attractive and can be used in applications such as energy conversion and storage applications, sensors, to mention two. In this work, the authors gave a brief historical overview of proton conductors, their structure and microstructure, and their correlation with conductivity. A perspective regarding the usage of these materials on low-temperature energy-related devices and sensors, among others, was given. Lastly, the authors emphasized the usage of proton conductors for humidity sensing applications and presented a resume of their efforts in developing humidity sensors using polyantimonic acid, a proton conductor. Their approach for enhancing the response is based on manipulating the type of binder and amount, from which they already obtained an almost linear response to humidity, with low aging and hysteresis.

**Author Contributions:** All authors contributed in equal parts to this article: Conceptualization, P.M.F. and E.S.A., Investigation and formal analysis, S.R.M., writing—original draft preparation, P.M.F., G.M.G.d.S. and E.S.A., writing—review and editing, G.M.G.d.S. and S.R.M. All authors have read and agreed to the published version of the manuscript.

**Funding:** This research is sponsored by national funds through FCT—Fundação para a Ciência e a Tecnologia, under the project UIDB/00285/2020, by LA/P/0112/2020, and by scholarship UI/BD/152285/2021 (<https://doi.org/10.54499/UI/BD/152285/2021>, accessed on 31 March 2024), and by Project APQ-1387-3.0322, Fundação de Apoio à Pesquisa do Estado de Pernambuco—FACEPE.

**Conflicts of Interest:** The authors declare no conflicts of interest. The funders had no role in the study's design; in the collection, analyses, or interpretation of data; in the writing of the manuscript; or in the decision to publish the results.

## References

1. Fabbri, E.; Pergolesi, D.; Traversa, E. Materials Challenges toward Proton-Conducting Oxide Fuel Cells: A Critical Review. *Chem. Soc. Rev.* **2010**, *39*, 4355. [[CrossRef](#)]
2. Norby, T. Proton Conduction in Solids: Bulk and Interfaces. *MRS Bull.* **2009**, *34*, 923–928. [[CrossRef](#)]
3. Sharma, S.; Pathak, D.; Dhiman, N.; Kumar, R.; Prashar, K.K.; Kahol, M.; Arora, N.; Sharma, V. Conductivity Study on Proton-Conducting Nanocomposite Plasticized Polymer Electrolytes: A Review. *Curr. Mater. Sci.* **2022**, *15*, 229–250. [[CrossRef](#)]
4. Gao, J.; Meng, Y.; Duffy, J.H.; Brinkman, K.S. Low-Temperature Protonic Ceramic Fuel Cells through Interfacial Engineering of Nanocrystalline BaCe<sub>0.7</sub>Zr<sub>0.1</sub>Y<sub>0.1</sub>Yb<sub>0.1</sub>O<sub>3-δ</sub> Electrolytes. *Adv. Energy Sustain. Res.* **2021**, *2*, 2100098. [[CrossRef](#)]
5. Park, H.J.; Roh, J.W. Protonic Conduction of Nanostructured Y-Doped BaZrO<sub>3</sub>. *J. Nanomater.* **2016**, *2016*, 8757305. [[CrossRef](#)]
6. Miyoshi, S.; Akao, Y.; Kuwata, N.; Kawamura, J.; Oyama, Y.; Yagi, T.; Yamaguchi, S. Low-Temperature Protonic Conduction Based on Surface Protonics: An Example of Nanostructured Ytria-Doped Zirconia. *Chem. Mater.* **2014**, *26*, 5194–5200. [[CrossRef](#)]
7. Gregori, G.; Shirpour, M.; Maier, J. Proton Conduction in Dense and Porous Nanocrystalline Ceria Thin Films. *Adv. Funct. Mater.* **2013**, *23*, 5861–5867. [[CrossRef](#)]
8. Takamura, H.; Takahashi, N. Electrical Conductivity of Dense Nanocrystalline Ceria under Humidified Atmosphere. *Solid State Ion.* **2010**, *181*, 100–103. [[CrossRef](#)]
9. Maglia, F.; Tredici, I.G.; Spinolo, G.; Anselmi-Tamburini, U. Low Temperature Proton Conduction in Bulk Nanometric TiO<sub>2</sub> Prepared by High-Pressure Field Assisted Sintering. *J. Mater. Res.* **2012**, *27*, 1975–1981. [[CrossRef](#)]
10. Wei, T.; Zhang, L.A.; Chen, Y.; Yang, P.; Liu, M. Promising Proton Conductor for Intermediate-Temperature Fuel Cells: Li<sub>13.9</sub>Sr<sub>0.1</sub>Zn(GeO<sub>4</sub>)<sub>4</sub>. *Chem. Mater.* **2017**, *29*, 1490–1495. [[CrossRef](#)]
11. Zhou, Y.; Guan, X.; Zhou, H.; Ramadoss, K.; Adam, S.; Liu, H.; Lee, S.; Shi, J.; Tsuchiya, M.; Fong, D.D.; et al. Strongly Correlated Perovskite Fuel Cells. *Nature* **2016**, *534*, 231–234. [[CrossRef](#)] [[PubMed](#)]
12. Meng, Y.; Gao, J.; Zhao, Z.; Amoroso, J.; Tong, J.; Brinkman, K.S. Review: Recent Progress in Low-Temperature Proton-Conducting Ceramics. *J. Mater. Sci.* **2019**, *54*, 9291–9312. [[CrossRef](#)]
13. Huang, Z.; Deng, J.; Wang, H.; Zhang, Y.; Duan, J.; Tang, Z.; Cao, Z.; Qi, J.; He, D.; Lu, T. Fast Low-Temperature Densification of Translucent Bulk Nanograin Gd<sub>2</sub>Zr<sub>2</sub>O<sub>7</sub> Ceramics with Average Grain Size below 10 Nm. *J. Alloys Compd.* **2020**, *830*, 154617. [[CrossRef](#)]
14. Bures, R.; Faberova, M.; Bircakova, Z.; Bednarcik, J.; Milyutin, V.; Petryshynets, I.; Kollar, P.; Füzér, J.; Dilyova-Hatrakova, M. High Pressure Compaction of Soft Magnetic Iron Powder. *Powder Technol.* **2023**, *421*, 118434. [[CrossRef](#)]
15. Choi, E.-Y.; Strathmann, H.; Park, J.-M.; Moon, S.-H. Characterization of Non-Uniformly Charged Ion-Exchange Membranes Prepared by Plasma-Induced Graft Polymerization. *J. Memb. Sci.* **2006**, *268*, 165–174. [[CrossRef](#)]
16. Syvertsen, G.E.; Estournès, C.; Fjeld, H.; Haugsrud, R.; Einarsrud, M.; Grande, T. Spark Plasma Sintering and Hot Pressing of Hetero-Doped LaNbO<sub>4</sub>. *J. Am. Ceram. Soc.* **2012**, *95*, 1563–1571. [[CrossRef](#)]
17. Kasyanova, A.V.; Zvonareva, I.A.; Tarasova, N.A.; Bi, L.; Medvedev, D.A.; Shao, Z. Electrolyte Materials for Protonic Ceramic Electrochemical Cells: Main Limitations and Potential Solutions. *Mater. Rep. Energy* **2022**, *2*, 100158. [[CrossRef](#)]
18. Kjølseth, C.; Fjeld, H.; Prytz, Ø.; Dahl, P.I.; Estournès, C.; Haugsrud, R.; Norby, T. Space-Charge Theory Applied to the Grain Boundary Impedance of Proton Conducting BaZr<sub>0.9</sub>Y<sub>0.1</sub>O<sub>3-δ</sub>. *Solid. State Ion.* **2010**, *181*, 268–275. [[CrossRef](#)]
19. Luo, J. Interfacial Engineering of Solid Electrolytes. *J. Mater.* **2015**, *1*, 22–32. [[CrossRef](#)]
20. Dzieciuch, M.A.; Weber, N. Dispositif Convertisseur d'énergie et Nouvel Électrolyte Solide Pour Ce Dispositif 1967, patent: FR1491673. Available online: <https://worldwide.espacenet.com/patent/search/family/027424861/publication/FR1491673A?q=FR1491673> (accessed on 31 March 2024).
21. Yao, Y.-F.Y.; Kummer, J.T. Ion Exchange Properties of and Rates of Ionic Diffusion in Beta-Alumina. *J. Inorg. Nucl. Chem.* **1967**, *29*, 2453–2475. [[CrossRef](#)]
22. Bruinink, J. Proton Migration in Solids. *J. Appl. Electrochem.* **1972**, *2*, 239–249. [[CrossRef](#)]
23. Glasser, L. Proton Conduction and Injection in Solids. *Chem. Rev.* **1975**, *75*, 21–65. [[CrossRef](#)]
24. Funke, K. Solid State Ionics: From Michael Faraday to Green Energy—The European Dimension. *Sci. Technol. Adv. Mater.* **2013**, *14*, 043502. [[CrossRef](#)]

25. Van Gool, W. Fast ion transport in solids, solid state batteries and devices. In Proceedings of the NATO Sponsored Advanced Study Institute on Fast Ion Transport in Solids, Solid State Batteries and Devices, Belgirate, Italy, 5–15 September 1972; van Gool, W., North Atlantic Treaty Organization, Scientific Affairs Division, Eds.; North Holland Pub. Co.: Amsterdam, The Netherlands; American Elsevier Pub. Co.: New York, NY, USA, 1973; ISBN 0444104321.
26. Farrington, G.C.; Briant, J.L.; Breiter, M.W.; Roth, W.L. Ionic Conductivity in  $\text{H}_3\text{O}^+$  Beta Alumina. *J. Solid. State Chem.* **1978**, *24*, 311–319. [[CrossRef](#)]
27. Colombar, P.; Boilot, J.-P.; Kahn, A.; Lucazeau, G. Structural Investigation of Protonic Conductor  $\text{NH}_4^+$  Beta Alumina and Stoichiometric  $\text{H}_3\text{O}^+$  Beta Alumina. *Nouv. J. Chim.* **1977**, *2*, 21–32.
28. Baffier, N.; Badot, J.; Colombar, P. Conductivity of  $\text{B}''$  and Ion Rich  $\beta$  Alumina. I.  $\text{H}^+(\text{H}_2\text{O})_n$  Compounds. *Solid State Ion* **1981**, *2*, 107–113. [[CrossRef](#)]
29. Baffier, N.; Badot, J.; Colombar, P. Protonic Conductivity of  $\text{B}''$  and Ion-Rich  $\beta$ -Alumina. II: Ammonium Compounds. *Solid State Ion* **1984**, *13*, 233–236. [[CrossRef](#)]
30. Lenfant, P.; Plas, D.; Ruffo, M.; Colombar, P.; Boilot, J.P. Ceramiques d'alumine  $\beta$  et de Ferrite  $\beta$  Pour Sonde a Protons. *Mater. Res. Bull.* **1980**, *15*, 1817–1827. [[CrossRef](#)]
31. Lundsgaard, J.S.; Brook, R.J. Mixed Conductivity of  $\beta$ -Alumina Electrolyte in Aqueous Concentration Cells. *J. Mater. Sci.* **1973**, *8*, 1519–1521. [[CrossRef](#)]
32. Lundsgaard, J.S.; Brook, R.J. The Use of  $\beta$ -Alumina Electrolyte in Gaseous Concentration Cells. *J. Mater. Sci.* **1974**, *9*, 2061–2062. [[CrossRef](#)]
33. Van Gool, W.; Huggins, R.A.; Roth, W.L.; Haven, Y.; Funke, K.; Whittingham, M.S.; Silbernagel, B.G.; Bacquet, G.; Dugas, J.; Powers, R.W.; et al. *Solid Electrolytes General Principles, Characterization, Materials, Applications*; Hagenmuller, P., van Gool, W., Eds.; Academic Press, Inc.: New York, NY, USA, 1978; ISBN 978-0-12-313360-1.
34. Stephen, P.; Howe, A. Proton Conductivity and Phase Relationship in Solid KOH between 248 and 406 °C. *Solid State Ion* **1980**, *1*, 461–471. [[CrossRef](#)]
35. Saalfeld, H.; Matthies, H.; Datta, S.K. Ein Neues Aluminiumoxidhydrat Mit  $\beta$ -Alumina Struktur. *Berichte Der Dtsch. Keram. Ges.* **1968**, *45*, 212–215.
36. Colombar, P.; Lucazeau, G.; Mercier, R.; Novak, A. Vibrational Spectra and Structure of  $\text{H}^+(\text{H}_2\text{O})_n$  B-alumina. *J. Chem. Phys.* **1977**, *67*, 5244–5251. [[CrossRef](#)]
37. Collongues, R.; Gourier, D.; Kahn, A.; Boilot, J.P.; Colombar, P.; Wicker, A.  $\beta$  Alumina, a Typical Solid Electrolyte: Latest Developments in Fundamental Approach and in Battery Utilization. *J. Phys. Chem. Solids* **1984**, *45*, 981–1013. [[CrossRef](#)]
38. Grubb, W.T., Jr. Fuel Cell 1959, patent: US 2913511. Available online: <https://patents.google.com/patent/US2913511A/en> (accessed on 31 March 2024).
39. Grubb, W.T.; Niedrach, L.W. Batteries with Solid Ion-Exchange Membrane Electrolytes: II. Low-Temperature Hydrogen-Oxygen Fuel Cells. *J. Electrochem. Soc.* **1960**, *107*, 131–135. [[CrossRef](#)]
40. Forrat, F.; Dauge, G.; Trévoux, P.; Danner, G.; Christen, M. Électrolyte Solide à Base de  $\text{AlLaO}_3$ . Application Aux Piles à Combustible. *C. R. Hebd. Seances Acad. Sci.* **1964**, *259*, 2813–2816.
41. Antonucci, P.L.; Aricò, A.S.; Cretì, P.; Ramunni, E.; Antonucci, V. Investigation of a Direct Methanol Fuel Cell Based on a Composite Nafion®-Silica Electrolyte for High Temperature Operation. *Solid State Ion* **1999**, *125*, 431–437. [[CrossRef](#)]
42. Perry, M.L.; Fuller, T.F. A Historical Perspective of Fuel Cell Technology in the 20th Century. *J. Electrochem. Soc.* **2002**, *149*, S59–S67. [[CrossRef](#)]
43. Takahashi, T.; Iwahara, H. Solid-State Ionics: Protonic Conduction in Perovskite Type Oxide Solid Solutions. *Rev. De Chim. Miner.* **1980**, *17*, 243–253.
44. Gavach, C.; Pourcelly, G. Applications of Perfluorinated Proton Conductors (Nafions). In *Proton Conductors Solids, Membranes and Gels—Materials and Devices*; Colombar, P., Ed.; Cambridge University Press: Cambridge, UK, 1992; pp. 487–498.
45. Lee, J.; D'Agostino, V.; Fried, R.; Diebold, E. Synthesis of Perfluorinated Ionomer Membranes for Electrochemical Cells. In *Proceedings of the Symposium on Diaphragms, Separators, and Ion-Exchange Membranes*; Van Zee, J.W., White, R.E., Kinoshita, K., Burney, H.S., Eds.; The Electrochemical Society Inc.: Pennington, South Africa, 1986; pp. 102–119.
46. Gruger, A.; Régis, A.; Schmatko, T.; Colombar, P. Nanostructure of Nafion® Membranes at Different States of Hydration: An IR and Raman Study. *Vib. Spectrosc.* **2001**, *26*, 215–225. [[CrossRef](#)]
47. Wolfe, W.R., Jr. Fuel Cell and Fuel Cell Electrode Comprising a Sulfurated Compound of Tungsten and Oxygen. 1968, patent: US 3615840. Available online: <https://patents.google.com/patent/US3615840A/en?q=US3615840A> (accessed on 31 March 2024).
48. Di Vona, M.L.; Knauth, P.; Ghobarkar, H.; Schäf, O.; Sgreccia, E.; Tosto, S.; Hempelmann, R.; Di Noto, V.; Giffin, G.A.; Vezzù, K.; et al. *Solid State Proton Conductors: Properties and Applications in Fuel Cells*, 1st ed.; Knauth, P., Di Vona, M.L., Eds.; John Wiley & Sons Ltd.: Hoboken, NJ, USA, 2012; ISBN 9780470669372.
49. Colombar, P. Proton Conductors and Their Applications: A Tentative Historical Overview of the Early Researches. *Solid State Ion* **2019**, *334*, 125–144. [[CrossRef](#)]
50. Cao, J.; Ji, Y.; Shao, Z. Perovskites for Protonic Ceramic Fuel Cells: A Review. *Energy Environ. Sci.* **2022**, *15*, 2200–2232. [[CrossRef](#)]
51. Potier, A.; Jones, D.J.; Rozière, J.; Colombar, P.; Novak, A.; Thomas, J.O.; Svare, I.; Dickens, P.G.; Chippindale, A.M.; Iwahara, H.; et al. *Proton Conductors: Solids, Membranes and Gels—Materials and Devices*; Colombar, P., Ed.; Cambridge University Press: Cambridge, UK, 1992; ISBN 9780521383172.



52. Hadži, D. Proton Transfers in Biological Mechanisms. *J. Mol. Struct.* **1988**, *177*, 1–21. [[CrossRef](#)]
53. Nagle, J.F.; Tristram-Nagle, S. Hydrogen Bonded Chain Mechanisms for Proton Conduction and Proton Pumping. *J. Membr. Biol.* **1983**, *74*, 1–14. [[CrossRef](#)] [[PubMed](#)]
54. Subramanian, M.A.; Roberts, B.D.; Clearfield, A. On the Proton Conductor  $(\text{H}_3\text{O})\text{Zr}_2(\text{PO}_4)_3$ . *Mater. Res. Bull.* **1984**, *19*, 1471–1478. [[CrossRef](#)]
55. Kreuer, K. Fast Proton Transport in Solids. *J. Mol. Struct.* **1988**, *177*, 265–276. [[CrossRef](#)]
56. Colomban, P.; Novak, A. Proton Transfer and Superionic Conductivity in Solids and Gels. *J. Mol. Struct.* **1988**, *177*, 277–308. [[CrossRef](#)]
57. Jaimez, E.; Hix, G.B.; Slade, R.C.T. A Phosphate–Phosphonate of Titanium(IV) Prepared from Phosphonomethyliminodiacetic Acid: Characterisation, n-Alkylamine Intercalation and Proton Conductivity. *Solid State Ion* **1997**, *97*, 195–201. [[CrossRef](#)]
58. Kreuer, K.-D. Proton Conductivity: Materials and Applications. *Chem. Mater.* **1996**, *8*, 610–641. [[CrossRef](#)]
59. Kreuer, K.D.; Münch, W.; Traub, U.; Maier, J. On Proton Transport in Perovskite-type Oxides and Plastic Hydroxides. *Berichte Bunsenges. Phys. Chem.* **1998**, *102*, 552–559. [[CrossRef](#)]
60. Asakura, Y.; Karasawa, H.; Sakagami, M.; Uchida, S. Relationships Between Corrosion Behavior of AISI 304 Stainless Steel in High-Temperature Pure Water and Its Oxide Film Structures. *Corrosion* **1989**, *45*, 119–124. [[CrossRef](#)]
61. Ramasubramanian, N.; Perovic, V.; Leger, M. Hydrogen Transport in the Oxide and Hydrogen Pickup by the Metal During Out- and In-Reactor Corrosion of Zr-2.5Nb Pressure Tube Material. In *Zirconium in the Nuclear Industry: Twelfth International Symposium*; Sabol, G.P., Moan, G.D., Eds.; ASTM International: West Conshohocken, PA, USA, 2000; pp. 853–876.
62. Scanu, T.; Guglielmi, J.; Colomban, P. Ion Exchange and Hot Corrosion of Ceramic Composites Matrices: A Vibrational and Microstructural Study. *Solid State Ion* **1994**, *70–71*, 109–120. [[CrossRef](#)]
63. Norby, T. Protonic Defects in Oxides and Their Possible Role in High Temperature Oxidation. *J. Phys. IV* **1993**, *03*, 99–106. [[CrossRef](#)]
64. Colomban, P. The Corrosion of Ceramic-Matrix Composites\*. *Mater. Sci. Forum* **1997**, *251–254*, 833–844. [[CrossRef](#)]
65. Colomban, P. Proton and Protonic Species: The Hidden Face of Solid State Chemistry. How to Measure H-Content in Materials? *Fuel Cells* **2013**, *13*, 6–18. [[CrossRef](#)]
66. Karlsson, M. Perspectives of Neutron Scattering on Proton Conducting Oxides. *Dalton Trans.* **2013**, *42*, 317–329. [[CrossRef](#)] [[PubMed](#)]
67. Kobzar, Y.; Oulyadi, H.; Marais, S.; Fatyeyeva, K. Advances in Nuclear Magnetic Resonance Spectroscopy: Case of Proton Conductive Materials. *J. Mater. Chem. A Mater.* **2023**, *11*, 6064–6089. [[CrossRef](#)]
68. Sakai, T.; Matsushita, S.; Hyodo, J.; Okuyama, Y.; Matsuka, M.; Ishihara, T.; Matsumoto, H. Effect of Doped Ceria Interlayer on Cathode Performance of the Electrochemical Cell Using Proton Conducting Oxide. *Electrochim. Acta* **2012**, *75*, 179–184. [[CrossRef](#)]
69. Oishi, M.; Akoshima, S.; Yashiro, K.; Sato, K.; Kawada, T.; Mizusaki, J. Defect Structure Analysis of Proton-Oxide Ion Mixed Conductor  $\text{BaCe}_{0.9}\text{Nd}_{0.1}\text{O}_{3-\delta}$ . *Solid State Ion* **2010**, *181*, 1336–1343. [[CrossRef](#)]
70. Tournié, A.; Ricciardi, P.; Colomban, P. Glass Corrosion Mechanisms: A Multiscale Analysis. *Solid State Ion* **2008**, *179*, 2142–2154. [[CrossRef](#)]
71. Jiang, S.P.; Li, Q. Protonic Ceramic Oxide Fuel Cells, Microbial Fuel Cells, and Biofuel Cells. In *Introduction to Fuel Cells—Electrochemistry and Materials*; Springer Nature Singapore Pte. Ltd.: Singapore, 2022; pp. 695–721. ISBN 978-981-10-7626-8.
72. Yan, S.; Yim, C.-H.; Pankov, V.; Bauer, M.; Baranova, E.; Weck, A.; Merati, A.; Abu-Lebdeh, Y. Perovskite Solid-State Electrolytes for Lithium Metal Batteries. *Batteries* **2021**, *7*, 75. [[CrossRef](#)]
73. Bouwmeester, H.J.M. Mixed Ionic-Electronic Conducting Membranes: Fundamentals and Challenges. In Proceedings of the ECerS2017—15th Conference & Exhibition of the European Ceramic Society, AKCongress, Budapest, Hungary, 9 July 2017; p. 406.
74. Zhang, W.; Hu, Y.H. Progress in Proton-conducting Oxides as Electrolytes for Low-temperature Solid Oxide Fuel Cells: From Materials to Devices. *Energy Sci. Eng.* **2021**, *9*, 984–1011. [[CrossRef](#)]
75. Naveen, M.V.; Soundarya, T.L.; Ravikiran, Y.T.; Krishnamurthy, G.; Anitha; Nagaraju, G. Facile Green Synthesis of Ni/NiO/MoO<sub>3</sub> Nanocomposite for Photocatalytic, Chromium (VI) Reduction, Electrochemical Dopamine (DA) and Humidity Sensor Applications. *Inorg. Chem. Commun.* **2024**, *160*, 111846. [[CrossRef](#)]
76. Shaheen, K.; Shah, Z.; Gulab, H.; Hanif, M.B.; Faisal, S.; Suo, H. Metal Oxide Nanocomposites as Anode and Cathode for Low Temperature Solid Oxide Fuel Cell. *Solid State Sci.* **2020**, *102*, 106162. [[CrossRef](#)]
77. Androš, L.; Jurić, M.; Popović, J.; Šantić, A.; Lazić, P.; Benčina, M.; Valant, M.; Brničević, N.; Planinić, P. Ba<sub>4</sub>Ta<sub>2</sub>O<sub>9</sub> Oxide Prepared from an Oxalate-Based Molecular Precursor—Characterization and Properties. *Inorg. Chem.* **2013**, *52*, 14299–14308. [[CrossRef](#)] [[PubMed](#)]
78. Huang, L.; Chen, X.; Wu, Y. The Interfacial Ionic Transport of Two-Dimensional ZnAl-Mixed Metal Oxides Nanocomposite. *J. Alloys Compd.* **2022**, *921*, 166118. [[CrossRef](#)]
79. Sun, S.; Tang, Q.; Zhang, K.; Wen, Y.; Billings, A.; Huang, K. A Focused Review on Structures and Ionic Conduction Mechanisms in Inorganic Solid-State Proton and Hydride Anion Conductors. *Mater. Adv.* **2023**, *4*, 389–407. [[CrossRef](#)]
80. Gao, J.; Liu, Z.; Akbar, M.; Gao, C.; Dong, W.; Meng, Y.; Jin, X.; Xia, C.; Wang, B.; Zhu, B.; et al. Efficiently Enhance the Proton Conductivity of YSZ-Based Electrolyte for Low Temperature Solid Oxide Fuel Cell. *Ceram. Int.* **2023**, *49*, 5637–5645. [[CrossRef](#)]
81. Tanabe, E.Y.; Assaf, E.M. Óxidos Do Tipo Perovskita Para Reação de Redução de NO Com CO. *Quim. Nova* **2009**, *32*, 1129–1133. [[CrossRef](#)]



82. Li, G.; Monroe, C.W. Transport of Secondary Carriers in a Solid Lithium-Ion Conductor. *Electrochim. Acta* **2021**, *389*, 138563. [CrossRef]
83. Yang, H.; Wang, C.-A.; Dong, Y. Energy Ceramic Design for Robust Battery Cathodes and Solid Electrolytes. *Adv. Powder Mater.* **2024**, *3*, 100185. [CrossRef]
84. Babar, Z.U.D.; Hanif, M.B.; Gao, J.-T.; Li, C.-J.; Li, C.-X. Sintering Behavior of BaCe<sub>0.7</sub>Zr<sub>0.1</sub>Y<sub>0.2</sub>O<sub>3-δ</sub> Electrolyte at 1150 °C with the Utilization of CuO and Bi<sub>2</sub>O<sub>3</sub> as Sintering Aids and Its Electrical Performance. *Int. J. Hydrogen Energy* **2022**, *47*, 7403–7414. [CrossRef]
85. Yu, M.; Feng, Q.; Liu, Z.; Zhang, P.; Zhu, X.; Mu, S. Recent Novel Fabrication Techniques for Proton-Conducting Solid Oxide Fuel Cells. *Crystals* **2024**, *14*, 225. [CrossRef]
86. Cheng, P.-C.; Lee, S.-W.; Lee, K.-R.; Setiawan, N.; Bhavanari, M.; Shen, C.-T.; Osman, N.; Tseng, C.-J. Carbon Resistant Ni1-*X*Cu<sub>*x*</sub>BCZY Anode for Methane-Fed Protonic Ceramic Fuel Cell. *Int. J. Hydrogen Energy* **2023**, *48*, 11455–11462. [CrossRef]
87. Lu, Y.; Shah, M.A.K.Y.; Mushtaq, N.; Yousaf, M.; Akbar, N.; Arshad, N.; Irshad, S. An Innovative Perovskite Oxide Enabling Improved Efficiency for Low-Temperature Ceramic Electrochemical Cells. *Fuel* **2024**, *367*, 131558. [CrossRef]
88. Duan, C.; Kee, R.; Zhu, H.; Sullivan, N.; Zhu, L.; Bian, L.; Jennings, D.; O'Hayre, R. Highly Efficient Reversible Protonic Ceramic Electrochemical Cells for Power Generation and Fuel Production. *Nat. Energy* **2019**, *4*, 230–240. [CrossRef]
89. An, H.; Lee, H.-W.; Kim, B.-K.; Son, J.-W.; Yoon, K.J.; Kim, H.; Shin, D.; Ji, H.-I.; Lee, J.-H. A 5 × 5 Cm<sup>2</sup> Protonic Ceramic Fuel Cell with a Power Density of 1.3 W Cm<sup>-2</sup> at 600 °C. *Nat. Energy* **2018**, *3*, 870–875. [CrossRef]
90. Le, L.Q.; Hernandez, C.H.; Zhu, L.; Ding, H.; Chmura, C.; Sullivan, N.P. Characterizing Stack Degradation in Proton-Conducting Ceramic Fuel Cells and Electrolyzers. *ECS Meet. Abstr.* **2020**, MA2020-01, 1614. [CrossRef]
91. Coetzee, C.J. Inorganic Ion Exchangers for Ion-Selective Electrodes. In *Inorganic Ion Exchangers in Chemical Analysis*; Qureshi, M., Varshney, K.G., Eds.; CRC Press: Boca Raton, FL, USA, 2019; pp. 143–175.
92. Silbernagel, R.; Martin, C.H.; Clearfield, A. Zirconium(IV) Phosphonate-Phosphates as Efficient Ion-Exchange Materials. *Inorg. Chem.* **2016**, *55*, 1651–1656. [CrossRef]
93. Colodrero, R.M.P.; Olivera-Pastor, P.; Cabeza, A.; Bazaga-García, M. Properties and Applications of Metal Phosphates and Pyrophosphates as Proton Conductors. *Materials* **2022**, *15*, 1292. [CrossRef]
94. Huang, W.; Komarneni, S.; Noh, Y.D.; Ma, J.; Chen, K.; Xue, D.; Xue, X.; Jiang, B. Novel Inorganic Tin Phosphate Gel: Multifunctional Material. *Chem. Commun.* **2018**, *54*, 2682–2685. [CrossRef] [PubMed]
95. Boilot, J.P.; Colomban, P.H.; Blanchard, N. Formation of Superionic Gels and Glasses by Low Temperature Chemical Polymerization. *Solid State Ion* **1983**, *9–10*, 639–643. [CrossRef]
96. Aoki, Y.; Harada, A.; Nakao, A.; Kunitake, T.; Habazaki, H. Percolative Proton Conductivity of Sol-Gel Derived Amorphous Aluminosilicate Thin Films. *Phys. Chem. Chem. Phys.* **2012**, *14*, 2735–2742. [CrossRef] [PubMed]
97. Comite, A. Preparation of Silica Membranes by Sol-Gel Method. In *Current Trends and Future Developments on (Bio-)Membranes*; Basile, A., Ghasemzadeh, A., Eds.; Elsevier B.V.: Amsterdam, The Netherlands, 2017; pp. 3–23. ISBN 9780444638670.
98. Fuhrhop, J.-H.; Blauer, G.; Weakley, T.J.R.; Novak, A. Large Molecules. In *Structure and Bonding*; Dunitz, J.D., Hemmerich, P., Holm, R.H., Ibers, J.A., Jørgensen, C.K., Neilands, J.B., Rinen, D., Williams, R.J.P., Eds.; Springer: Berlin/Heidelberg, Germany, 1974; Volume 18.
99. Thi, M.P. Microprobe Study of Enhanced Raman Scattering Effect on WO<sub>3</sub>/Ag Thin Films. *Chem. Phys. Lett.* **1985**, *115*, 130–133.
100. Zhong, Q.; Colbow, K. Hydrogen and Lithium Intercalation in Cs<sub>*x*</sub>WO<sub>3</sub>. *Thin Solid Films* **1991**, *196*, 305–313. [CrossRef]
101. Slade, R.C.T.; Hirst, P.R.; West, B.C. Ammonium-Ion Motions in the Hexagonal Tungsten Trioxide Framework. A Neutron Scattering Study of the Bronze (NH<sub>4</sub>)<sub>0.22</sub>WO<sub>3</sub> and of [(NH<sub>4</sub>)<sub>2</sub>O]<sub>0.085</sub>WO<sub>3</sub>. *J. Mater. Chem.* **1991**, *1*, 281–288. [CrossRef]
102. Genin, C.; Driouiche, A.; Gérard, B.; Figlarz, M. Hydrogen Bronzes of New Oxides of the WO<sub>3</sub>-MoO<sub>3</sub> System with Hexagonal, Pyrochlore and ReO<sub>3</sub>-Type Structures. *Solid State Ion* **1992**, *53–56*, 315–323. [CrossRef]
103. Dupont, L.; Larcher, D.; Portemer, F.; Figlarz, M. Synthesis and Characterization of New Oxide Hydrates H<sub>*x*</sub>(V<sub>*x*</sub>Mo<sub>1-*x*</sub>)O<sub>3</sub>·0.3H<sub>2</sub>O and H<sub>0.27</sub>(V<sub>0.27</sub>W<sub>0.73</sub>)O<sub>3</sub>·1/3H<sub>2</sub>O. *J. Solid State Chem.* **1996**, *121*, 339–349. [CrossRef]
104. Whittingham, M.S. Hydrogen Motion in Oxides: From Insulators to Bronzes. *Solid State Ion* **2004**, *168*, 255–263. [CrossRef]
105. Huo, L.; Zhao, H.; Mauvy, F.; Fourcade, S.; Labrugere, C.; Pouchard, M.; Grenier, J.C. Synthesis and Mixed Conductivity of Ammonium Tungsten Bronze with Tunneling Structures. *Solid State Sci.* **2004**, *6*, 679–688. [CrossRef]
106. Upasen, S.; Batocchi, P.; Mauvy, F.; Slodczyk, A.; Colomban, P. Chemical and Structural Stability of La<sub>0.6</sub>Sr<sub>0.4</sub>Co<sub>0.2</sub>Fe<sub>0.8</sub>O<sub>3-δ</sub> Ceramic vs. Medium/High Water Vapor Pressure. *Ceram. Int.* **2015**, *41*, 14137–14147. [CrossRef]
107. Upasen, S.; Batocchi, P.; Mauvy, F.; Slodczyk, A.; Colomban, P. Protonation and Structural/Chemical Stability of Ln<sub>2</sub>NiO<sub>4+δ</sub> Ceramics vs. H<sub>2</sub>O/CO<sub>2</sub>: High Temperature/Water Pressure Ageing Tests. *J. Alloys Compd.* **2015**, *622*, 1074–1085. [CrossRef]
108. MacDiarmid, A.G.; Chiang, J.C.; Richter, A.F.; Somasiri, N.L.D.; Epstein, A.J. Polyaniline: Synthesis and Characterization of the Emeraldine Oxidation State by Elemental Analysis. In *Conducting Polymers, Special Applications*; Alcácer, L., Ed.; D. Reidel Publishing Company: Dordrecht, The Netherlands, 1987; pp. 105–120. ISBN 978-94-009-3907-3.
109. Cao, Y.; Smith, P.; Heeger, A.J. Counter-Ion Induced Processibility of Conducting Polyaniline and of Conducting Polyblends of Polyaniline in Bulk Polymers. *Synth. Met.* **1992**, *48*, 91–97. [CrossRef]
110. Hinrichs, R.; Régis, A.; Gruger, A.; Colomban, P. Pressure—Temperature-Induced Conductivity in Polyaniline Base and Salts. *Synth. Met.* **1996**, *81*, 227–231. [CrossRef]

111. Hatchett, D.W.; Josowicz, M.; Janata, J. Acid Doping of Polyaniline: Spectroscopic and Electrochemical Studies. *J. Phys. Chem. B* **1999**, *103*, 10992–10998. [[CrossRef](#)]
112. El Khalki, A.; Gruger, A.; Colombar, P. Bulk–Surface Nanostructure and Defects in Polyaniline Films and Fibres. *Synth. Met.* **2003**, *139*, 215–220. [[CrossRef](#)]
113. Folch, S.; Gruger, A.; Régis, A.; Colombar, P. Optical and Vibrational Spectra of Sols/Solutions of Polyaniline: Water as Secondary Dopant. *Synth. Met.* **1996**, *81*, 221–225. [[CrossRef](#)]
114. Gao, H.; Lian, K. Proton Conducting Heteropoly Acid Based Electrolyte for High Rate Solid Electrochemical Capacitors. *J. Electrochem. Soc.* **2011**, *158*, A1371–A1378. [[CrossRef](#)]
115. Oesten, R.; Huggins, R.A. Proton Conduction in Oxides: A Review. *Ionics* **1995**, *1*, 427–437. [[CrossRef](#)]
116. Meng, X.; Wang, H.-N.; Song, S.-Y.; Zhang, H.-J. Proton-Conducting Crystalline Porous Materials. *Chem. Soc. Rev.* **2017**, *46*, 464–480. [[CrossRef](#)]
117. Chiodelli, G.; Maglia, F.; Anselmi-Tamburini, U.; Munir, Z.A. Characterization of Low Temperature Protonic Conductivity in Bulk Nanocrystalline Fully Stabilized Zirconia. *Solid State Ion* **2009**, *180*, 297–301. [[CrossRef](#)]
118. De Grotthuss, C.J.T. Sur La Décomposition de l’eau et Des Corps Qu’elle Tient En Dissolution à l’aide de l’électricité Galvanique. *Ann. Chim.* **1806**, *58*, 54–74.
119. Bhagat, M.S.; Mungray, A.K.; Mungray, A.A. Recent Advances in Osmotic Microbial Fuel Cell Technology: A Review. *J. Indian Chem. Soc.* **2022**, *99*, 100552. [[CrossRef](#)]
120. Park, H.J.; Kwak, C.; Lee, K.H.; Lee, S.M.; Lee, E.S. Interfacial Protonic Conduction in Ceramics. *J. Eur. Ceram. Soc.* **2009**, *29*, 2429–2437. [[CrossRef](#)]
121. Avila-Paredes, H.J.; Barrera-Calva, E.; Anderson, H.U.; De Souza, R.A.; Martin, M.; Munir, Z.A.; Kim, S. Room-Temperature Protonic Conduction in Nanocrystalline Films of Yttria-Stabilized Zirconia. *J. Mater. Chem.* **2010**, *20*, 6235. [[CrossRef](#)]
122. Guo, X. On the Degradation of Zirconia Ceramics during Low-Temperature Annealing in Water or Water Vapor. *J. Phys. Chem. Solids* **1999**, *60*, 539–546. [[CrossRef](#)]
123. Kurapova, O.Y.; Faia, P.M.; Zaripov, A.A.; Pazheltsev, V.V.; Glukharev, A.A.; Konakov, V.G. Electrochemical Characterization of Novel Polyantimonic-Acid-Based Proton Conductors for Low- and Intermediate-Temperature Fuel Cells. *Appl. Sci.* **2021**, *11*, 11877. [[CrossRef](#)]
124. Miyoshi, S.; Akao, Y.; Kuwata, N.; Kawamura, J.; Oyama, Y.; Yagi, T.; Yamaguchi, S. Water Uptake and Conduction Property of Nano-Grained Yttria-Doped Zirconia Fabricated by Ultra-High Pressure Compaction at Room Temperature. *Solid State Ion* **2012**, *207*, 21–28. [[CrossRef](#)]
125. Jing, Y.; Matsumoto, H.; Aluru, N.R. Mechanistic Insights into Hydration of Solid Oxides. *Chem. Mater.* **2018**, *30*, 138–144. [[CrossRef](#)]
126. Raz, S.; Sasaki, K.; Maier, J.; Riess, I. Characterization of Adsorbed Water Layers on Y<sub>2</sub>O<sub>3</sub>-Doped ZrO<sub>2</sub>. *Solid State Ion* **2001**, *143*, 181–204. [[CrossRef](#)]
127. Contescu, C.; Contescu, A.; Schwarz, J.A. Thermodynamics of Proton Binding at the Alumina/Aqueous Solution Interface. A Phenomenological Approach. *J. Phys. Chem.* **1994**, *98*, 4327–4335. [[CrossRef](#)]
128. Morimoto, T.; Nagao, M.; Tokuda, F. Relation between the Amounts of Chemisorbed and Physisorbed Water on Metal Oxides. *J. Phys. Chem.* **1969**, *73*, 243–248. [[CrossRef](#)]
129. Anderson, J.H.; Parks, G.A. Electrical Conductivity of Silica Gel in the Presence of Adsorbed Water. *J. Phys. Chem.* **1968**, *72*, 3662–3668. [[CrossRef](#)]
130. Malavasi, L.; Fisher, C.A.J.; Islam, M.S. Oxide-Ion and Proton Conducting Electrolyte Materials for Clean Energy Applications: Structural and Mechanistic Features. *Chem. Soc. Rev.* **2010**, *39*, 4370. [[CrossRef](#)] [[PubMed](#)]
131. Yamada, M.; Wei, M.; Honma, I.; Zhou, H. One-Dimensional Proton Conductor under High Vapor Pressure Condition Employing Titanate Nanotube. *Electrochem. Commun.* **2006**, *8*, 1549–1552. [[CrossRef](#)]
132. Haile, S.M.; West, D.L.; Campbell, J. The Role of Microstructure and Processing on the Proton Conducting Properties of Gadolinium-Doped Barium Cerate. *J. Mater. Res.* **1998**, *13*, 1576–1595. [[CrossRef](#)]
133. Kim, S.; Avila-Paredes, H.J.; Wang, S.; Chen, C.-T.; De Souza, R.A.; Martin, M.; Munir, Z.A. On the Conduction Pathway for Protons in Nanocrystalline Yttria-Stabilized Zirconia. *Phys. Chem. Chem. Phys.* **2009**, *11*, 3035. [[CrossRef](#)] [[PubMed](#)]
134. Wilkins, R.W.T.; Mateen, A. The Spectroscopic Study of Oxonium Ions in Mineral. *Am. Miner.* **1974**, *59*, 811–819.
135. Lippert, E.; Schuster, P.; Janoschek, R.; Brickmann, J.; Weidemann, E.; Hofacker, G.L.; Marechal, Y.; Ratner, M.; Perram, J.W.; Jonsson, P.-G.; et al. *The Hydrogen Bond: Dynamics, Thermodynamics and Special Systems*, 1st ed.; Sandorfy, C., Zundel, G., Schuster, P., Eds.; North-Holland Publishing Company: Amsterdam, The Netherlands, 1976.
136. Bauer, B.; Jones, D.J.; Rozière, J.; Tchicaya, L.; Alberti, G.; Casciola, M.; Massinelli, L.; Peraio, A.; Besse, S.; Ramunni, E. Electrochemical Characterisation of Sulfonated Polyetherketone Membranes. *J. New Mater. Electrochem. Syst.* **2000**, *3*, 93–98.
137. Savadogo, O. Emerging Membranes for Electrochemical Systems: (I) Solid Polymer Electrolyte Membranes for Fuel Cell Systems. *J. New Mater. Electrochem. Syst.* **1998**, *1*, 47–66. [[CrossRef](#)]
138. Kobayashi, T.; Rikukawa, M.; Sanui, K.; Ogata, N. Proton-Conducting Polymers Derived from Poly(Ether-Etherketone) and Poly(4-Phenoxybenzoyl-1,4-Phenylene). *Solid State Ion* **1998**, *106*, 219–225. [[CrossRef](#)]

139. Kerres, J.; Ullrich, A.; Haring, T. New Ionomer Membranes and Their Fuel Cell Application 1. Preparation and Characterization. In Proceedings of the 3rd International Symposium on New Materials for Electrochemical Systems, Montreal, QC, Canada, 4–8 July 1999; p. 230.
140. Alberti, G.; Casciola, M.; Palombari, R.; Peraio, A. Protonic Conductivity of Layered Zirconium Phosphonates Containing -SO<sub>3</sub>H Groups. II. Ac Conductivity of Zirconium Alkyl-Sulphophenyl Phosphonates in the Range 100–200 °C, in the Presence or Absence of Water Vapour. *Solid State Ion* **1992**, *58*, 339–344. [[CrossRef](#)]
141. Alberti, G.; Boccali, L.; Casciola, M.; Massinelli, L.; Montoneri, E. Protonic Conductivity of Layered Zirconium Phosphonates Containing—SO<sub>3</sub>H Groups. III. Preparation and Characterization of  $\gamma$ -Zirconium Sulfoaryl Phosphonates. *Solid State Ion* **1996**, *84*, 97–104. [[CrossRef](#)]
142. Yaroshenko, F.; Lupitskaya, Y.; Ulyanov, M.; Burmistrov, V.; Filonenko, E.; Galimov, D.; Uchaev, D.; Rubtsova, E. Synthesis, Microstructure, and Electrophysical Properties of Surface-Modified Polyantimonic Acid Nanoparticles. *J. Electrochem. Sci. Eng.* **2023**, *13*, 911–921. [[CrossRef](#)]
143. Yaroshenko, F.A.; Burmistrov, V.A. Proton Conductivity of Polyantimonic Acid Studied by Impedance Spectroscopy in the Temperature Range 370–480 K. *Inorg. Mater.* **2015**, *51*, 783–787. [[CrossRef](#)]
144. Alberti, G.; Costantino, U.; Casciola, M.; Ferroni, S.; Massinelli, L.; Staiti, P. Preparation, Characterization and Proton Conductivity of Titanium Phosphate Sulphophenylphosphonate. *Solid State Ion* **2001**, *145*, 249–255. [[CrossRef](#)]
145. Debbarma, L.; Panwar, V.; Khanduri, P.; Panwar, L.S. Development of Flexible PVDF/PAMPS Polyelectrolyte Proton Conductive Membrane. *Mater. Today Proc.* **2020**, *26*, 1776–1779. [[CrossRef](#)]
146. ul Imaan, D.; Mir, F.Q.; Ahmad, B. In-Situ Preparation of PSSA Functionalized ZWP/Sulfonated PVDF Composite Electrolyte as Proton Exchange Membrane for DMFC Applications. *Int. J. Hydrogen Energy* **2022**, *47*, 41347–41358. [[CrossRef](#)]
147. Jensen, S.H.; Graves, C.; Mogensen, M.; Wendel, C.; Braun, R.; Hughes, G.; Gao, Z.; Barnett, S.A. Large-Scale Electricity Storage Utilizing Reversible Solid Oxide Cells Combined with Underground Storage of CO<sub>2</sub> and CH<sub>4</sub>. *Energy Environ. Sci.* **2015**, *8*, 2471–2479. [[CrossRef](#)]
148. Tarasova, N.; Bedarkova, A. Advanced Proton-Conducting Ceramics Based on Layered Perovskite BaLaInO<sub>4</sub> for Energy Conversion Technologies and Devices. *Materials* **2022**, *15*, 6841. [[CrossRef](#)]
149. Xing, Y.; Zhu, B.; Hong, L.; Xia, C.; Wang, B.; Wu, Y.; Cai, H.; Rauf, S.; Huang, J.; Asghar, M.I.; et al. Designing High Interfacial Conduction beyond Bulk via Engineering the Semiconductor–Ionic Heterostructure CeO<sub>2– $\delta$</sub> /BaZr<sub>0.8</sub>Y<sub>0.2</sub>O<sub>3</sub> for Superior Proton Conductive Fuel Cell and Water Electrolysis Applications. *ACS Appl. Energy Mater.* **2022**, *5*, 15373–15384. [[CrossRef](#)] [[PubMed](#)]
150. Tarasova, N.; Bedarkova, A.; Animitsa, I. Novel Pr-Doped BaLaInO<sub>4</sub> Ceramic Material with Layered Structure for Proton-Conducting Electrochemical Devices. *Appl. Sci.* **2023**, *13*, 1328. [[CrossRef](#)]
151. Tarasova, N.; Bedarkova, A.; Animitsa, I. Proton Transport in the Gadolinium-Doped Layered Perovskite BaLaInO<sub>4</sub>. *Materials* **2022**, *15*, 7351. [[CrossRef](#)] [[PubMed](#)]
152. Alberti, G.; Palombari, R. All Solid State Hydrogen Sensors Based on Pellicular  $\alpha$ -Zirconium Phosphate as a Protonic Conductor. *Solid State Ion* **1989**, *35*, 153–156. [[CrossRef](#)]
153. Alberti, G.; Casciola, M.; Chieli, S.; Palombari, R. Use of Solid State Protonic Conductors for Oxygen Potentiometric Sensor at Room Temperature. *Solid State Ion* **1991**, *46*, 183–186. [[CrossRef](#)]
154. Alberti, G.; Casciola, M.; Palombari, R. Amperometric Sensor for Carbon Monoxide Based on Solid State Protonic Conduction. *Solid State Ion* **1993**, *61*, 241–244. [[CrossRef](#)]
155. Alberti, G.; Cherubini, F.; Palombari, R. Amperometric Solid-State Sensor for NO and NO<sub>2</sub> Based on Protonic Conduction. *Sens. Actuators B Chem.* **1996**, *37*, 131–134. [[CrossRef](#)]
156. Zhao, H.; Liu, L.; Lin, X.; Dai, J.; Liu, S.; Fei, T.; Zhang, T. Proton-Conductive Gas Sensor: A New Way to Realize Highly Selective Ammonia Detection for Analysis of Exhaled Human Breath. *ACS Sens.* **2020**, *5*, 346–352. [[CrossRef](#)] [[PubMed](#)]
157. Dai, J.; Qi, R.; Tu, J.; Zhao, H.; Liu, S.; Fei, T.; Zhang, T. Humidity Sensor Preparation by In Situ Click Polymerization. *IEEE Electron. Device Lett.* **2018**, *39*, 1234–1237. [[CrossRef](#)]
158. Liang, X.; Li, B.; Wang, M.; Wang, J.; Liu, R.; Li, G. Effective Approach to Promoting the Proton Conductivity of Metal–Organic Frameworks by Exposure to Aqua–Ammonia Vapor. *ACS Appl. Mater. Interfaces* **2017**, *9*, 25082–25086. [[CrossRef](#)]
159. Iwahara, H.; Uchida, H.; Ogaki, K.; Nagato, H. Nernstian Hydrogen Sensor Using BaCeO<sub>3</sub>-Based, Proton-Conducting Ceramics Operative at 200°–900 °C. *J. Electrochem. Soc.* **1991**, *138*, 295–299. [[CrossRef](#)]
160. Okuyama, Y.; Nagamine, S.; Nakajima, A.; Sakai, G.; Matsunaga, N.; Takahashi, F.; Kimata, K.; Oshima, T.; Tsuneyoshi, K. Proton-Conducting Oxide with Redox Protonation and Its Application to a Hydrogen Sensor with a Self-Standard Electrode. *RSC Adv.* **2016**, *6*, 34019–34026. [[CrossRef](#)]
161. Luo, J.; Dziubla, T.; Eitel, R. A Low Temperature Co-Fired Ceramic Based Microfluidic Clark-Type Oxygen Sensor for Real-Time Oxygen Sensing. *Sens. Actuators B Chem.* **2017**, *240*, 392–397. [[CrossRef](#)]
162. Wang, X.; Qin, T.; Bao, S.-S.; Zhang, Y.-C.; Shen, X.; Zheng, L.-M.; Zhu, D. Facile Synthesis of a Water Stable 3D Eu-MOF Showing High Proton Conductivity and Its Application as a Sensitive Luminescent Sensor for Cu<sup>2+</sup> Ions. *J. Mater. Chem. A Mater.* **2016**, *4*, 16484–16489. [[CrossRef](#)]
163. Zhang, M.; Tan, W.; Wu, X.; Wan, C.; Wen, C.; Feng, L.; Zhang, F.; Qu, F. A Dual-Functional Cuprum Coordination Framework for High Proton Conduction and Electrochemical Dopamine Detection. *Microchim. Acta* **2024**, *191*, 67. [[CrossRef](#)]

164. Zhou, F.; Lim, H.N.; Ibrahim, I.; Endot, N.A.; Malek, E.A.; Gowthaman, N.S.K. Simultaneous Electrochemical Detection of Dopamine and Uric Acid via Au@Cu-Metal Organic Framework. *Chempluschem* **2024**, *89*, e202300686. [[CrossRef](#)] [[PubMed](#)]
165. Yadav, D.; Shrivastava, A.; Sircar, A.; Dhorajiya, P.; Muniya, A.; Bhattacharyay, R.P. Development and Performance Evaluation of Sr<sub>2</sub>CeO<sub>4</sub>—SrCe<sub>0.85</sub>Y<sub>0.15</sub>O<sub>3- $\infty$</sub>  Based Electrochemical Hydrogen Isotopes Sensor. *Fusion Eng. Des.* **2024**, *200*, 114189. [[CrossRef](#)]
166. Rahman, M.H.; Rashed, M.A.; Nayem, N.I.; Rahaman, M.A.; Ahmed, J.; Faisal, M.; Jalalah, M.; Harraz, F.A. Nanogold-Decorated Reduced Graphene Oxide/Chitosan Composite for Electrochemical Sensing of N-Acetyl-4-Aminophenol. *Mater. Chem. Phys.* **2024**, *314*, 128915. [[CrossRef](#)]
167. Abid, K.; Iannazzo, D.; Celesti, C.; Khaskhoussi, A.; Foti, A.; Maalej, R.; Gucciardi, P.G.; Neri, G. A Novel 2D-GO@WS<sub>2</sub> Electrochemical Platform for the Determination of Thiram Fungicide. *J. Environ. Sci.* **2024**, *136*, 226–236. [[CrossRef](#)]
168. Iwahara, H.; Uchida, H.; Kondo, J. Galvanic Cell-Type Humidity Sensor Using High Temperature-Type Proton Conductive Solid Electrolyte. *J. Appl. Electrochem.* **1983**, *13*, 365–370. [[CrossRef](#)]
169. Katahira, K.; Matsumoto, H.; Iwahara, H.; Koide, K.; Iwamoto, T. A Solid Electrolyte Steam Sensor with an Electrochemically Supplied Hydrogen Standard Using Proton-Conducting Oxides. *Sens. Actuators B Chem.* **2000**, *67*, 189–193. [[CrossRef](#)]
170. Cobb, L.J.; Kumar, R.V.; Fray, D.J. A Novel Humidity Sensor Using Yb-Doped SrCeO<sub>3</sub> Ionic Conductor with a Au-Pd Filter. *Ionics* **1996**, *2*, 231–234. [[CrossRef](#)]
171. Miao, J.; Chen, Y.; Li, Y.; Cheng, J.; Wu, Q.; Ng, K.W.; Cheng, X.; Chen, R.; Cheng, C.; Tang, Z. Proton Conducting Polyoxometalate/Polypyrrole Films and Their Humidity Sensing Performance. *ACS Appl. Nano Mater.* **2018**, *1*, 564–571. [[CrossRef](#)]
172. Zou, J.; Zhang, K.; Zhang, Q. Giant Humidity Response Using a Chitosan-Based Protonic Conductive Sensor. *IEEE Sens. J.* **2016**, *16*, 8884–8889. [[CrossRef](#)]
173. Farahani, H.; Wagiran, R.; Urban, G.A. Investigation of Room Temperature Protonic Conduction of Perovskite Humidity Sensors. *IEEE Sens. J.* **2021**, *21*, 9657–9666. [[CrossRef](#)]
174. Kalyakin, A.S.; Danilov, N.A.; Volkov, A.N. Determining Humidity of Nitrogen and Air Atmospheres by Means of a Protonic Ceramic Sensor. *J. Electroanal. Chem.* **2021**, *895*, 115523. [[CrossRef](#)]
175. Medvedev, D.; Kalyakin, A.; Volkov, A.; Demin, A.; Tsiakaras, P. Electrochemical Moisture Analysis by Combining Oxygen- and Proton-Conducting Ceramic Electrolytes. *Electrochem. Commun.* **2017**, *76*, 55–58. [[CrossRef](#)]
176. Hatakeyama, K.; Karim, M.R.; Ogata, C.; Tateishi, H.; Funatsu, A.; Taniguchi, T.; Koinuma, M.; Hayami, S.; Matsumoto, Y. Proton Conductivities of Graphene Oxide Nanosheets: Single, Multilayer, and Modified Nanosheets. *Angew. Chem. Int. Ed.* **2014**, *53*, 6997–7000. [[CrossRef](#)]
177. Guo, L.; Jiang, H.-B.; Shao, R.-Q.; Zhang, Y.-L.; Xie, S.-Y.; Wang, J.-N.; Li, X.-B.; Jiang, F.; Chen, Q.-D.; Zhang, T.; et al. Two-Beam-Laser Interference Mediated Reduction, Patterning and Nanostructuring of Graphene Oxide for the Production of a Flexible Humidity Sensing Device. *Carbon N. Y.* **2012**, *50*, 1667–1673. [[CrossRef](#)]
178. Mendes, S.; Kurapova, O.; Faia, P.; Pazheltsev, V.; Zaripov, A.; Konakov, V. Polyantimonic Acid-Based Materials Evaluated as Moisture Sensors at Ambient Temperature. *J. Solid. State Electrochem.* **2023**, *27*, 611–625. [[CrossRef](#)]
179. Mendes, S.; Kurapova, O.; Faia, P. Enhancing Polyantimonic-Based Materials' Moisture Response with Binder Content Tuning. *Chemosensors* **2023**, *11*, 423. [[CrossRef](#)]

**Disclaimer/Publisher's Note:** The statements, opinions and data contained in all publications are solely those of the individual author(s) and contributor(s) and not of MDPI and/or the editor(s). MDPI and/or the editor(s) disclaim responsibility for any injury to people or property resulting from any ideas, methods, instructions or products referred to in the content.